Low Temperature Catalytic Ethanol Conversion Over Ceria-Supported Platinum, Rhodium, and Tin-Based Nanoparticle Systems

Thesis by

Eugene Leo Draine Mahmoud

In Partial Fulfillment of the Requirements for the Degree of Engineer

California Institute of Technology
Pasadena, California

(Defended 2010)

بِسْمِ اللَّهِ الرَّحْمَٰنِ الرَّحِيمِ

Abstract

Due to the feasibility of ethanol production in the United States, ethanol has become more attractive as a fuel source and a possible energy carrier within the hydrogen economy. Ethanol can be stored easily in liquid form, and can be internally pre-formed prior to usage in low temperature (200^{o}C – 400^{o}C) solid acid and polymer electrolyte membrane fuel cells. However, complete electrochemical oxidation of ethanol remains a challenge. Prior research of ethanol reforming at high temperatures (> 400^{o}C) has identified several metallic and oxide-based catalyst systems that improve ethanol conversion, hydrogen production, and catalyst stability. In this study, ceria-supported platinum, rhodium, and tin-based nanoparticle catalyst systems will be developed and analyzed in their performance as low-temperature ethanol reforming catalysts for fuel cell applications.

Metallic nanoparticle alloys were synthesized with ceria supports to produce the catalyst systems studied. Gas phase byproducts of catalytic ethanol reforming were analyzed for temperature-dependent trends and chemical reaction kinetic parameters. Results of catalytic data indicate that catalyst composition plays a significant role in low-temperature ethanol conversion. Analysis of byproduct yields demonstrate how ethanol steam reforming over bimetallic catalyst systems (platinum-tin and rhodium-tin) results in higher hydrogen selectivity than was yielded over single-metal catalysts. Additionally, oxidative steam reforming results reveal a correlation between catalyst composition, byproduct yield, and ethanol conversion. By analyzing the role of temperature and reactant composition on byproduct yields from ethanol reforming, this study also proposes how these parameters may contribute to optimal catalytic ethanol reforming.

Table of Contents

1 Introduction and Theory

Steam reforming is a thermochemical process in which large hydrocarbon molecules are broken down into hydrogen gas (H_2), smaller oxides, and hydrocarbons. Steam reforming of natural resources is the primary process for the industrial production of hydrogen gas in the world. About 50% of the world's production of hydrogen gas and 95% of hydrogen gas production in the United States is generated from steam reforming of natural gas [13]. When synthesized at a large scale, steam reforming typically employs a catalyst and high temperatures (> 600^{o}C), and is the most energy efficient and cost efficient means of producing hydrogen gas.

Steam reforming of alcohols has been proposed as a primary means of hydrogen production for fuel cell devices. Fuel cells are advantageous as energy conversion devices for several reasons. They are more energy efficient than Carnot-limited combustion engines. When using hydrogen gas as a fuel source, the only byproduct produced is water vapor (H_2O). Also, the performance of low temperature (< 100^{o}C) proton exchange membrane fuel cells is suitable for a wide range of mobile applications. Identifying an appropriate source for hydrogen production will solidify the role of fuel cells in the energy marketplace.

As a means to address concerns over energy security, sustainability of energy sources, and global climate change, using a non-petroleum-based energy carrier for fuel cells is critical [11]. Ethanol (CH_3CH_2OH) is attractive as a feedstock for hydrogen gas production, in part, because of its ample production domestically—composing 99% of biofuel production in the United States. Also, ethanol can be produced renewably, it is low in toxicity, it can be easily transported, and it has a relatively high energy density. Thus the catalytic reforming of ethanol provides a plausible means of hydrogen gas production for the forthcoming fuel cell industry. For certain

intermediate temperature (200°C–400°C) fuel cells, internal reforming of ethanol could improve reforming efficiency while removing the challenges of hydrogen gas storage from the fuel cell system. The objective of this section of the thesis is to delineate the different approaches and reactions incorporated in ethanol reforming, to discuss the advantages of oxide-supported metal catalysts for hydrogen gas production, and to discuss how multi-component catalysts may offer improvements in catalytic ethanol reforming.

1.1 Thermochemistry of Ethanol Reforming

The main approaches to ethanol reforming for fuel cells are external reforming, integrated reforming, and internal reforming [23]. In external reforming, the conversion to hydrogen takes place in a separate reactor, and the resultant fuel is fed into the fuel channels. These catalytic systems may be able to benefit from the fuel cell stack's waste heat, but in general, they operate as technologically mature independent systems. Integrated reforming involves some arrangement in which the membrane electrode assembly (MEA) and the reformer are alternatively arranged within the fuel cell stack. This approach benefits from a close thermal contact between MEA and the reformer. Internal reforming requires the direct incorporation of a reformate layer into either the fuel channel and/or anode. This approach ensures maximum thermal efficiency and a coupling of all reforming byproducts into the anode's electrochemical reactions.

Several reaction pathways are available to ethanol reforming, and the thermodynamics of these reactions are presented in the remainder of this section.

1.1.1 Steam Reforming

The most desirable form of the steam reforming (SR) reaction is endothermic and produces only hydrogen and carbon dioxide (CO_2).

$CH_3CH_2OH(l) + 3\ H_2O(l) \rightarrow 6H_2(g) + 2CO_2(g)$ $\Delta H_{298} = +347.5\ kJ\ mol^{-1}$ (1)

The two other steam reforming reactions produce less desirable byproducts—carbon monoxide (CO) and methane (CH_4)—in exchange with hydrogen or carbon dioxide [3].

$CH_3CH_2OH(l) + H_2O(l) \rightarrow 4\ H_2(g) + 2CO(g)$ $\Delta H_{298} = +341.7\ kJ\ mol^{-1}$ (2)

$CH_3CH_2OH(l) + 2\ H_2(g) \rightarrow 2\ CH_4(g) + H_2O(g)$ $\Delta H_{298} = -114.0\ kJ\ mol^{-1}$ (3)

Given that reactions (1) and (2) are endothermic and increase the amount of moles in the system, SR conditions at high temperatures (> 700°C) will favor hydrogen production and the methane producing reaction (3) will be less favorable. In the comparison of reactions (1) and (2), the higher (3:1) molar ratio of water-to-ethanol in reaction (1) favors the production of CO_2 as opposed to CO.

1.1.2 Partial Oxidation

When a sub-stoichiometric amount of oxygen gas (O_2) is present in the reactant mixture with ethanol, an exothermic reaction produces carbon dioxide and hydrogen.

$CH_3CH_2OH(l) + 1.5\ O_2(g) \rightarrow 3\ H_2(g) + 2CO_2(g)$ $\Delta H_{298} = -510.0\ kJ\ mol^{-1}$ (4)

Less than ideal reactions that may occur during partial oxidation (PO) conditions would result in the production of carbon monoxide and/or water vapor [28].

$CH_3CH_2OH(l) + 0.5\ O_2(g) \rightarrow 3\ H_2(g) + 2CO(g)$ $\Delta H_{298} = +55.9\ kJ\ mol^{-1}$ (5)

$CH_3CH_2OH(l) + 2\ O_2(g) \rightarrow 3\ H_2O(g) + 2CO(g)$ $\Delta H_{298} = -669.6\ kJ\ mol^{-1}$ (6)

PO allows for ethanol reforming at lower temperatures (i.e. without heat input) and without the presence of steam. However, reaction (4) inherently exhibits a lower hydrogen selectivity—moles of hydrogen produced per mole of ethanol consumed—then is does reaction (1).

1.1.3 Oxidative Steam Reforming

Oxidative steam reforming (OSR) occurs when steam reforming and the partial oxidation reaction conditions are coupled. The OSR reaction, also known as autothermal reforming reaction, results in the production of hydrogen and carbon dioxide with only a small change in the system's enthalpy.

$CH_3CH_2OH(l) + 1.8\ H_2O(l) + 0.6\ O_2(g) \rightarrow 4.8\ H_2(g) + 2CO_2(g)$ $\Delta H_{298} = +4.5\ kJ\ mol^{-1}$ (7)

The hydrogen selectivity for reaction (7) is slightly lower than that of reaction (1). However, the slight change in the system's enthalpy would make this equation more sustainable at low temperatures.

1.1.4 Additional Ethanol Reforming Reactions

Besides the primary reactions described above, other likely reactions include ethanol decomposition, water gas shift (WGS), ethanol dehydrogenation, ethanol dehydration, and methanation reactions [33].

$CH_3CH_2OH(l) \rightarrow CO + CH_4 + H_2$ $\Delta H_{298} = +91.8\ kJ\ mol^{-1}$ (8)

$CH_3CH_2OH(l) \rightarrow 0.5\ CO_2 + 1.5\ CH_4$ $\Delta H_{298} = -31.7\ kJ\ mol^{-1}$ (9)

$CO + H_2O \rightarrow CO_2 + H_2$ $\Delta H_{298} = -41.1\ kJ\ mol^{-1}$ (10)

$CH_3CH_2OH(l) \rightarrow H_2 + CH_3CHO(l)$ $\Delta H_{298} = +84.8\ kJ\ mol^{-1}$ (11)

$CH_3CH_2OH(l) \rightarrow C_2H_4(g) + H_2O(g)$ $\Delta H_{298} = +87.6\ kJ\ mol^{-1}$ (12)

$CO + 3H_2 \rightarrow CH_4 + H_2O$ $\Delta H_{298} = -206\ kJ\ mol^{-1}$ (13)

Due to the many possible reaction pathways that are available for ethanol steam reforming, it is important to identify which reactions are the most likely to occur and to catalytically promote the reactions that most strongly favor the production of hydrogen and carbon dioxide. Reaction (9) is strongly favored at low temperatures (~ 200^{o}C), and may dominate over reactions (1) and (2). The water-gas-shift reaction (10) strongly favors the conversion of carbon monoxide to carbon dioxide in the presence of steam [11]. This reaction is an important step in purifying steam reforming byproducts, particularly because the production of carbon monoxide can result in the poisoning or deactivation of certain metal catalysts typically used in reformers and fuel cell anodes. Carbon formation is also a reaction that may result from the presence of carbon-containing byproducts. Coking may result from the Boudouard reaction, the decomposition of methane and hydrocarbon polymerization.

$2CO \rightarrow C(s) + CO_2$ $\Delta H_{298} = -172$ kJ mol^{-1} (14)

$CH_4 \rightarrow 2H_2 + C(s)$ $\Delta H_{298} = +74.6$ kJ mol^{-1} (15)

C2H4 → polymers → coke (16)

Designing a catalyst system in which these coking reactions are limited is crucial for the development of a stable and active ethanol reforming catalyst. The challenge has led to increasing research in the development of stable and active catalysts for ethanol reforming.

1.2 Metal Catalysts for Ethanol Reforming

Typically, ethanol reforming is carried out at high temperatures (> 600^{o}C). An ideal catalyst system for low-temperature ethanol reforming would be stable, highly selective to H_2, and composed of accessible materials. Noble metal catalysts have typically been used in industrial catalytic reformers to produce hydrogen from ethanol.

Platinum-based catalysts are well-known for being active in the electrochemical oxidation of alcohols. Ethanol reforming to hydrogen over platinum (Pt) is promoted via ethanol decomposition (8) and ethanol dehydration (11, 12) [7, 8, 15, 20, 21, 39]. However, ethanol reforming at lower temperatures (< 500^{o}C) generally leads to catalyst deactivation with acetaldehyde and methane as the primary byproducts. In particular, the low selectivity to hydrogen in favor of carbon monoxide suggests that the platinum surface promotes the reverse water gas shift reaction. Palladium-based catalysts tend to promote similar reaction byproducts, although activity at low temperatures is lower than platinum [14].

Rhodium (Rh) has been shown to be the most active, stable, and resistant to sintering amongst oxide-supported noble metals catalysts for ethanol reforming [12]. Rhodium is an efficient metal catalyst that is active in breaking the carbon–carbon (C-C) and hydrocarbon (H-C) bonds of possible intermediates—such as acetaldehyde and oxametallacycles—during ethanol steam reforming [22]. As shown in Figure 1, an oxametallacycle refers to the five-member adsorbed complex formed by the insertion of a metal dimer into one of the C-O bonds of an ethylene oxide molecule (C_2H_4O). The stability of these structures favors the breaking of the C-C bond, particularly in an oxidizing atmosphere [28]. Given that oxametallacycles are more energetically favorable on the surface of rhodium than adsorbed acetaldehyde, ethanol decomposition on rhodium is more likely to promote C-C bond rupture. However, hydrogen selectivity over rhodium catalysts varies with fabrication, loading, and oxide support. Oxide support is particularly critical at low temperatures (< 500^{o}C) [10], at which methane and carbon monoxide production are significant amongst reforming products. This suggests that Rh alone is not catalytically active enough to efficiently produce hydrogen at low temperatures.

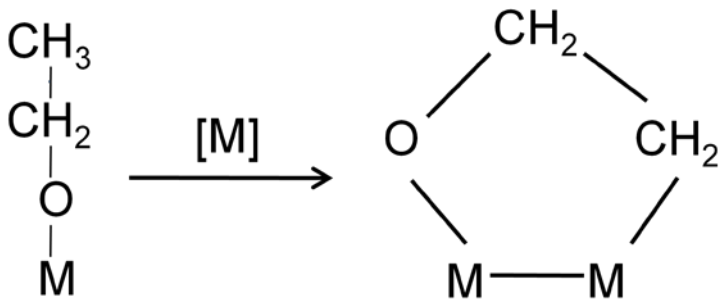

Figure 1: Formation of an adsorbed oxametallacycle from an adsorbed ethylene oxide molecule

Amongst non-noble metals, nickel catalysts have also been used in ethanol reforming because of their known activity in oxidation reactions, their low-temperature activity in dehydrogenation reactions, and their low cost [30, 31]. Cobalt catalysts have demonstrated peak hydrogen selectivity at 450°C with a $CeZrO_4$ support [19] and are active in the breaking of the carbon-carbon bond. However, particle size and coking are factors that limit the stability for both of these metal catalysts at low temperatures.

1.3 Oxides as Catalysts and Metal Catalyst Supports

Despite the prevalent role of metals in catalytic reactions, studies of oxide materials have demonstrated their ability to act as catalysts and to enhance the performance and stability of metal catalysts [3]. The choice of a support material can favor other secondary reactions—such as water splitting into hydroxyl (OH) groups and hydrogen radicals—and can promote the migration of these reactive species toward the metal particles. Support materials can also aid in the dispersion and thermal stability of metal particles.

Cerium oxide or ceria (CeO_2) has garnered interest in the material science community for its ability to participate in homogeneous catalytic reactions [1, 13, 27, 32], such as three-way catalysis (TWC) and fluid catalytic cracking. The stoichiometric form of ceria is a face-centered cubic cell with a fluorite structure. When treated in a reducing atmosphere at elevated

temperatures, a continuum of oxygen-deficient non-stoichiometric oxides are formed. These suboxides are readily reoxidized to CeO_2 in an oxidizing environment. The ability of CeO_2 to release and store oxygen allows for improved performance from nearby catalysts—such as in the water-gas shift reaction (10) and ethanol dehydrogenation (11). As a metal support, oxides and metals have a synergistic relationship. Precious metals promote the reduction and oxidation of CeO_2, while CeO_2 stabilizes the dispersion of the precious metal and resists sintering. Other commonly used supports in steam reforming reactions include aluminum oxide (Al_2O_3) [2, 40], magnesium oxide (MgO), titanium oxide (TiO_2) [24,29], zinc oxide (ZnO) [4], and zirconium oxide (ZrO_2) [5, 19].

1.4 Multi-Component Catalyst Systems

In an effort to enhance catalytic activity, catalyst development has been increasingly employing smaller catalyst particle size and metal alloys instead of single metal catalysts. The bifunctional theory of electrocatalysis was proposed by Watanabe and colleagues [35—37] to account for the change in electrocatalytic activity of these multi-component systems. This theory is presupposed on the mixture of electrocatalysts—with different adsorption properties—on the atomic scale. Watanabe's work demonstrated how oxidation of organic molecules over platinum was improved by the atomic level addition of other electrocatalysts (i.e., gold, ruthenium) that could access lower energy pathways for the adsorption of reactive species. Effectively, one metal acts as sites for organic species and another metal acts as sites for oxygen-containing species. Complex reactions involving various species and reaction pathways will thus occur more efficiently at metal interfaces.

Given the unique performance of multi-phase nanoparticles catalyst systems, there has been an increasing effort by researchers to identify and describe the varied and synergistic roles of metal

and oxide catalyst materials. DeSouza and colleagues conducted a study of ethanol oxidation over a $PtRh_x$ alloy electrode [9]. Using differential electrochemical mass spectroscopy (DEMS) and Fourier transform infrared spectroscopy (FTIR), their work demonstrated that the addition of Rh to a Pt catalyst increases the selectivity towards the complete oxidation of ethanol to CO_2, while decreasing selectivity to acetaldehyde. Ethanol oxidation requires C-H bond and C-C bond dissociation, in addition to CO-O bond coupling. DeSouza's work suggests that because Pt has a relatively low bond energy for CO and O adsorption, Pt and $PtRh_x$ catalysts are more likely than Rh to have a lower CO_2 activation energy. A linear sweep voltammetric study of adsorbed CO suggests that Rh ad-atoms modify the electrocatalytic properties of Pt to promote the partial oxidation of CO [8]. While in a bimetallic system, Rh continues to play the role one would expect it to perform in a single catalyst system. A mechanistic study of $PtRh_x$ confirms that while Rh allows for the formation of adsorbed oxametallacycles, and thus carbon-carbon bond decomposition, an additional metal (Pt, Pd) is necessary for efficient hydrogen production [28]. In addition, the presence of a CeO_2 support also favors the dehydrogenation of ethanol to acetaldehyde.

Platinum-tin alloys also participate in the oxidation of ethanol and catalytic promotion of CO partial oxidation. Dissociative adsorption of water molecules on tin (Sn) allows for OH species to interact in the dissociative adsorption of ethanol, into CO_2 and CH_3COOH [34]. Additionally, numerical calculations suggest that the CO oxidation potential on $PtSn_x$ is lower then the oxidation potential on Pt. However, this has yet to be experimentally confirmed. An electrochemical characterization of $PtSn_x$ and $PtSn_xO_y$ electrodes by Jiang and colleagues [16] shows that ethanol oxidation and hydrogen selectivity is more favorable on $PtSn_xO_y$. One possible explanation is that tin oxide particles near Pt particles act as oxygen donor sites for the CO-O bond coupling.

Recent studies of ternary catalyst systems continue to offer new insights into the roles that Pt, Rh, and Sn play in ethanol reforming. A study of ethanol oxidation over a carbon-supported $Pt_6Sn_3Ru_1$ showed high performance relative to the ethanol oxidizing ability of other binary and ternary catalyst systems considered [38]. The presence of the PtSn phase and the SnO_2 were identified as active structures in C-C bond dissociation. Ribeiro and colleagues considered the addition of iridium [25] and tungsten [26] to a carbon-supported PtSn binary system. Both materials enhanced the electrocatalytic activity of PtSn, possibly through some synergistic structural arrangement with Sn, or by limiting ethanol adsorption in favor of oxygen containing species. Several studies of $PtRh_xSn_y$ electrodes system have touted their performance as ethanol oxidation catalysts [6, 17]. However, further studies of $PtRh_x$, $PtSn_x$, and $PtRh_xSn_y$ catalysts as low-temperature ethanol reformers will be needed to identify the optimal material for low-temperature reforming and fuel cell conditions.

1.5 Proposed Work

The ideal ethanol reforming catalyst will be highly selective to hydrogen, with a low selectivity to methane, acetaldehyde, and a minimal production of CO and other large hydrocarbon complexes while operating in reactor at low temperatures ($200^{o}C$–$400^{o}C$) and atmospheric pressures. Designing an optimal catalyst for hydrogen production from ethanol requires consideration of the catalyst fabrication technique, proper choice of catalyst components, support structure, and careful definition of the reforming environment. Catalyst design is particularly critical in the low temperature regime, where reaction kinetics often plays a role larger than thermodynamics. In this study, ceria-supported, 5%-weight Pt, Rh, $PtSn_x$, and $RhSn_x$ catalysts will be fabricated and analyzed in their performance as low-temperature ethanol reforming catalysts for fuel cell applications. We will discuss trends in ethanol reforming over these catalyst systems, identify reaction kinetic parameters for the production of the ethanol

reforming byproducts that we detect, and propose future studies to help identify an optimal ethanol reforming catalyst.

2 Experimental Approach

The catalyst materials used were composed of Pt_xSn_{1-x} or Rh_xSn_{1-x} nanoparticles with x = 1, 0.9 and 0.8 on a porous ceria support (95% by weight). The catalysts were fabricated at Occidental College by Marc Sells, under the supervision of Dr. Adrian Hightower. The mass of each catalyst sample studied is shown in Table 1. A modified version of reverse micelles synthesis was used to produce platinum, rhodium, and tin nanoparticles with diameters ranging from 1–10 nm. Nanoparticles were dispersed on the surface ceria supports, and the resulting cermet powder was washed, dried, mixed with quartz sand (10 parts by volume), and mounted into a 0.8 inch diameter plug flow reactor—as shown by the diagram in Figure 2. The catalyst material was sandwiched in between two fine porous quartz cylinders—one fused to the end of the reactor tube and the other slip fit into the inlet side of the tube. This setup ensures that inlet gases pass through the catalyst system at a known rate. A thermocouple was mounted through the inlet-side quartz cylinder to monitor the catalyst sample temperature, and a horizontal Carbolite tube furnace was used to heat the reactor.

Table 1: Masses of catalyst material used in ethanol reforming studies

	Rh	$Rh_{0.9}Sn_{0.1}$	$Rh_{0.8}Sn_{0.2}$	Pt	$Pt_{0.9}Sn_{0.1}$	$Pt_{0.8}Sn_{0.2}$
Catalyst mass used	217 mg	235.4mg	223.5 mg	220.4 mg	254mg	263.5 mg

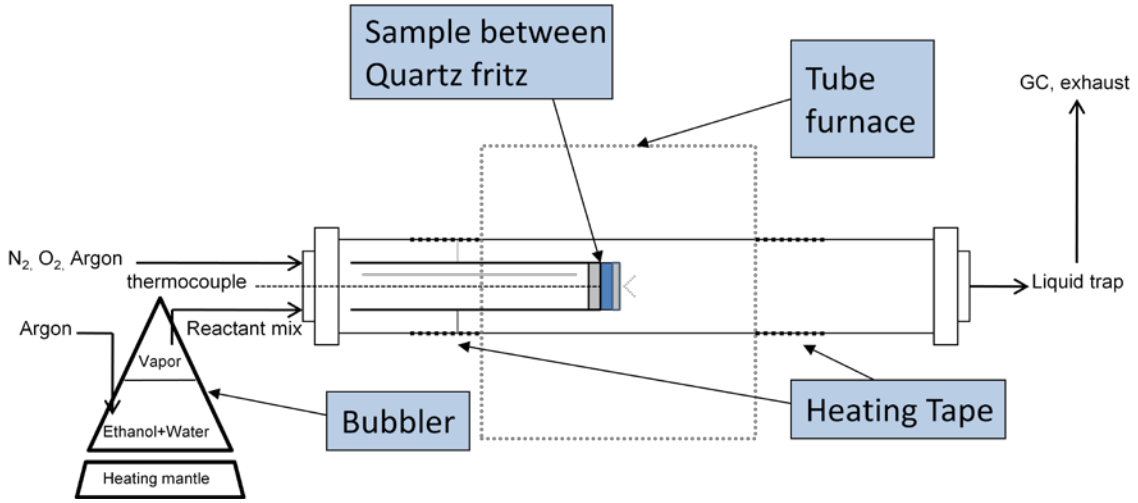

Figure 2: A schematic of the tube furnace reactor setup

Reactant gases and reactant products were ported through the valves at the reactor's end caps. The water-to-ethanol gas phase molar ratio of the reactant was set to a desired value by premixing the liquids in a bubbler, and heating the mixture to a predetermined temperature (≈ 70°C). A rotameter was used to flow argon through the bubbler as a means of transporting a vapor mixture of steam and ethanol to the catalyst. Additional rotameters were used to transport nitrogen, oxygen, and additional argon to the catalyst bed within the tube furnace reactor. The measurement of the volume of reactants used and the accuracy of the rotameters were the primary sources of systematic error observed with results of this study. A liquid vaporizer was considered for the transport of ethanol, but this method could not yield the large reactant flow rates required. Flow meters typically operate in much larger ranges than we required, and flow rates produced were less accurate.

After installing the catalyst in the reactor tube, the catalyst bed was preheated to 400°C at 5°C per minute under flowing argon for two hours, and then reduced under a 2% H_2 flow at a rate of 120 mL/min for 10 hours at the same temperature. Prior to testing the catalyst, the reactor tube outside of the tube furnace was heated to 200°C by heating tape. The inlet line from the

bubbler, the outlet line to the GC, and the reactor end caps were heated to a temperature between 70°C and 100°C. The reducing flow was removed from the reactor at least an hour prior to the catalytic studies and gas chromatography was used to confirm that argon was the only gas present. Catalytic studies were allowed 30 minutes to reach equilibrium prior to the initial recording of data. Results were averaged over a 30 minute period.

A liquid trap was maintained at a set temperature (i.e. 30°C) and was installed at the reactor outlet and was used to condense saturated ethanol vapor, saturated water vapor, and any other saturated vapor byproducts. The remaining gas phase products entered the Varian CP-4900 gas chromatograph with Molecular Sieve 5A and Porapak Q columns running on argon carrier gas. Product gas compositions (H_2, CO, CO_2, CH_4, C_2H_4, C_2H_6, O_2, and CH_3CHO) were obtained directly. Ethanol vapor was also detected by the gas chromatograph. This ethanol vapor is the amount of unsaturated ethanol vapor at the outlet of the reactor, and thus was not condensed in the liquid trap. Thus, the product gas composition of ethanol was determined by correlating the amount of ethanol gas vapor detected to the known vapor pressure of ethanol at the liquid trap's temperature. Alternatively, an absorption tube was installed at the reactor outlet to capture all catalytic products. The tube was then purged with helium gas and analyzed for gas and liquid phase products using the GC/MS setup (Hewlett-Packard 6890 GC -5973 MSD System) in Caltech's Environmental Analysis Center under the supervision of Dr. Nathan Dalleska. Kinetic reaction parameters reported were obtained by numerical fitting of experimental data in the Origin 6.1 software package.

3 Results and Data Analysis

Steam reforming (SR) of ethanol was studied using a reactant mixture with a molar water-to-ethanol ratio of 3:1, which corresponded to the ideal stoichiometric ratio for the production of hydrogen (1). The ratio of catalyst weight to reactant flow rate was 7.8 (kg / m/sec). Ethanol vapor, steam, and argon flow rates were set at 10, 31, and 120 sccm, respectively. These conditions produced a Gas Space Hourly Velocity (GHSV)—defined as the milliliters of reactant flow per hour per milliliters of catalyst used—of approximately 5000 hr^{-1} at 400^{o}C over ceria-supported Pt. The total amount of ethanol converted was the difference between the ethanol flow rate at the inlet and the detected ethanol flow rate at the outlet. While hydrogen selectivity would be maximized at lower reactant feed rates (and lower GSHV), low reactant conversion (≈ 25%) and a smaller slope in molar-selectivity-to-GSHV is required to accurately study kinetic reaction data in the differential regime of the reactor. Figure 3 shows a plot of GSHV versus ethanol conversion and hydrogen selectivity using steam reforming conditions over a ceria-supported platinum catalyst. At a GSHV of 5000 hr^{-1} the steam reforming reaction should occur in the differential regime of the reactor. Systemic error for steam reforming measurements is represented by error bars of 5.4%. Product gases will be presented in units of molar selectivity, defined in this study as the ratio of moles produced for a certain byproduct to the moles of ethanol converted.

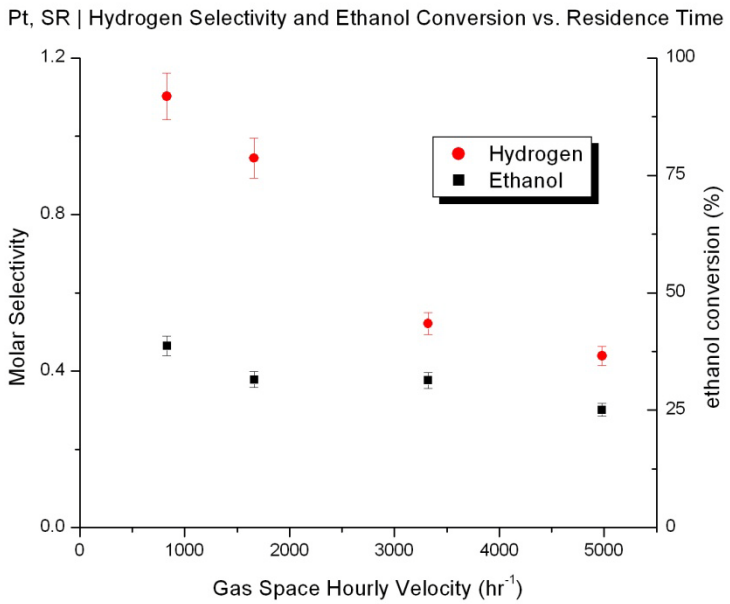

Figure 3: Plot of hydrogen selectivity and ethanol conversion versus reactant residence time over a Pt/CeO_2 catalyst. Temperature is 400°C, and the reactant mixture has a water-to-ethanol ratio of 3:1.

Oxidative steam reforming (OSR) of ethanol was studied using a water-to-ethanol-to-oxygen molar ratio of 1.8:1.0:0.6, which corresponds to the optimal stoichiometric ratio for the production of hydrogen (7). The ratio of catalyst mass to reactant flow rate was 6.1 (kg / m/sec). Ethanol vapor, steam, oxygen, and argon flow rates were set to 15.7, 28.2, 9.4, and 120 sccm, respectively. These settings produced a GSHV of approximately 6400 hr^{-1} at 400°C over ceria-supported Pt. Ethanol conversion at these conditions is around 40% (see Figure 4), but hydrogen selectivity is relatively low and appears independent of residence time at these conditions. Thus, OSR at a GSHV of 6400 hr^{-1} should fall within the differential regime of the reactor and allow for accurate calculation of kinetic information. Systemic error for oxidative steam reforming measurements is represented by error bars of 7.1%.

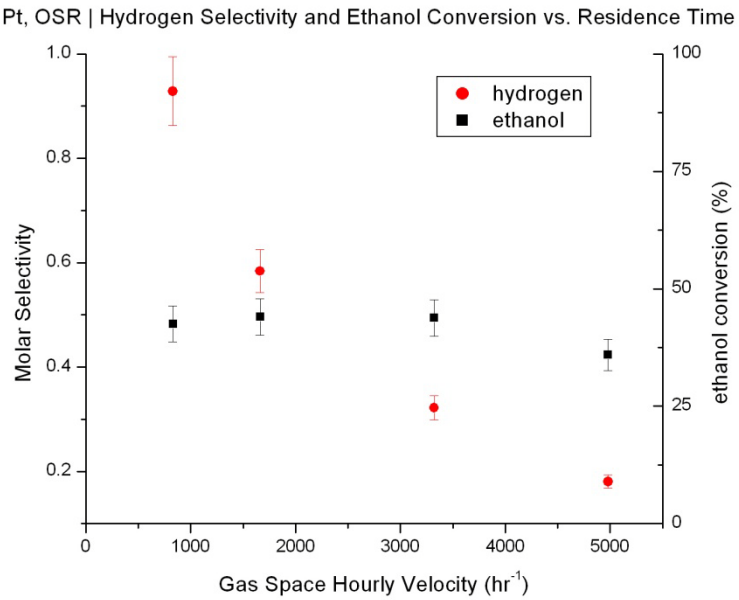

Figure 4: Plot of hydrogen selectivity and ethanol conversion versus reactant residence time over a Pt/CeO_2 catalyst. Temperature is 400°C, and the reactant mixture has a water-to-ethanol-to-oxygen molar ratio of 1.8:1.0:0.6.

Reforming byproducts for steam reforming and oxidative steam reforming were studied at 50°C intervals between 200°C and 400°C over ceria-supported platinum, rhodium, platinum-tin, and rhodium-tin catalysts using the flow rates information given above. For results using different reactant flow conditions, reactant composition will be noted in subsequent sections. Reforming byproducts were analyzed for trends resulting from the varying the stoichiometric reactant compositions. The steam, ethanol or oxygen concentration in the reactant mixture was varied, while the remaining reactant components were held constant. During these studies, temperature was held constant at 400°C.

3.1 Steam Reforming

3.1.1 Rh_xSn_{1-x}/CeO_2, (x = 1, 0.9, 0.8)

Selected results of the ethanol steam reforming studies over Rh-based catalysts are presented in Figures 5–10. Ethanol conversion is one of the primary means for comparing the performance of a catalyst, as it correlates the efficiency of the complex reaction mechanisms that produce the byproducts detected. The conversion of ethanol varied between 20% and 40%, generally increasing with increasing temperature over Rh, while slightly decreasing with increasing temperature over Rh_8Sn_2. Ethanol reforming over Rh_9Sn_1 produced the highest ethanol conversion (30–35%) amongst Rh-based catalysts. Selectivity for hydrocarbons and carbon dioxide remained minimal (< 0.1) for all Rh-based catalyst systems and temperatures, although selectivity for these products was enhanced by increasing temperature. As shown in Figure 8, selectivity to smaller hydrocarbons (methane, ethylene) and carbon dioxide was higher with steam reforming over the Rh catalyst, while selectivity to acetaldehyde (ethanal/CH_3CHO) was higher with steam reforming over Rh-Sn catalyst systems. The primary products observed in these steam reforming studies were hydrogen and carbon monoxide. Carbon monoxide selectivity increased with increasing temperature across all catalyst systems studies (0.1–0.2). Hydrogen selectivity increased with temperature for the Rh and the Rh_8Sn_2 catalyst. Selectivity increased more slowly and exponentially for the Rh_9Sn_1 catalyst. At 400°C, production and selectivity to hydrogen was highest for Rh_8Sn_2, followed by Rh_9Sn_1 and Rh. The Rh_9Sn_1 catalyst had the lowest hydrogen selectivity in the group at temperatures below 350°C, while the Rh_8Sn_2 catalyst had the highest selectivity above 300°C. Finally, by calculating the difference between the moles of carbon in the reactants and the moles of carbon in the products, the moles of undetected carbon-containing products can be estimated. This difference can be attributed to the selectivity for carbon-containing products that were not detected by our experiment (i.e.,

benzene, etc.), and this selectivity has been represented with other reforming products in the figures below. Selectivity to undetected carbon-containing products for all the Rh-based catalyst systems decreased with increasing temperatures, and this decrease likely corresponds strongly to the production of other byproducts.

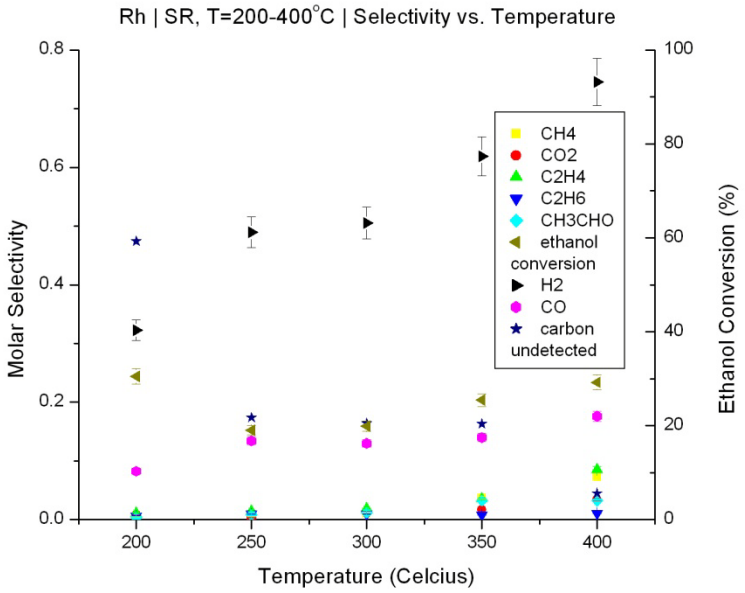

Figure 5: Plot of molar selectivity and ethanol conversion versus temperature over Rh/CeO_2 from steam reforming

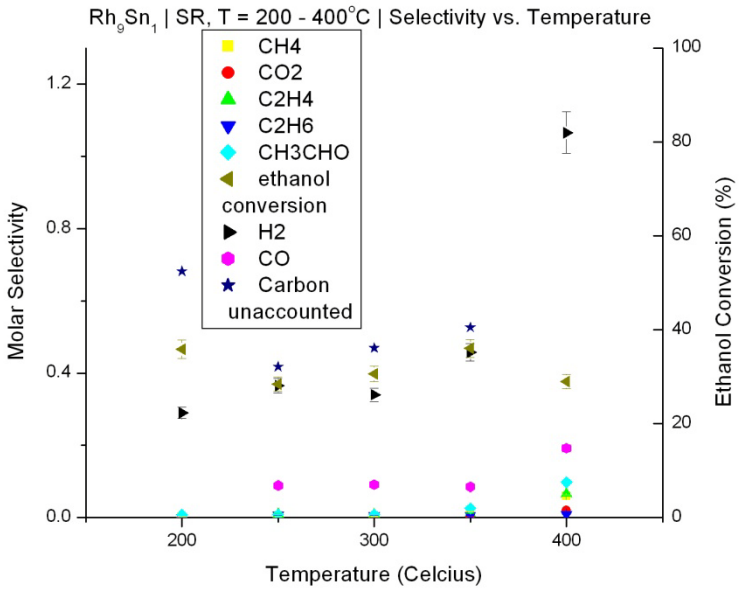

Figure 6: Plot of molar selectivity and ethanol conversion versus temperature over Rh_9Sn_1/CeO_2 from steam reforming

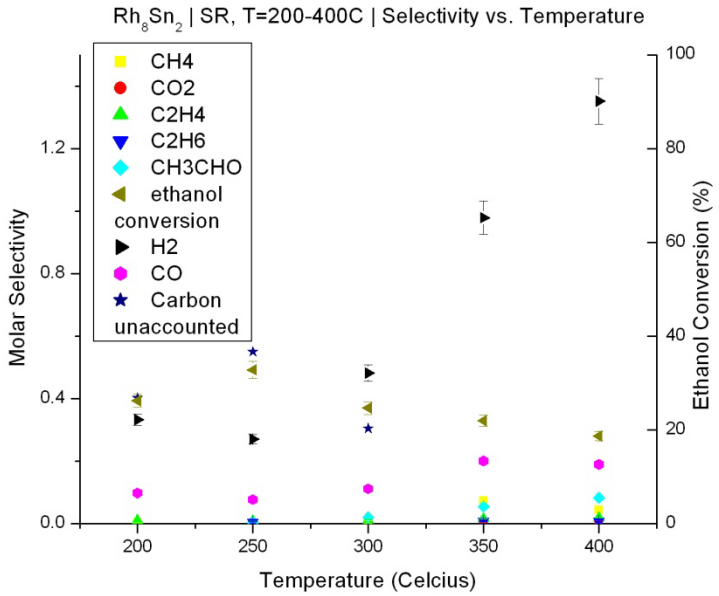

Figure 7: Plot of molar selectivity and ethanol conversion versus temperature over Rh_8Sn_2/CeO_2 from steam reforming

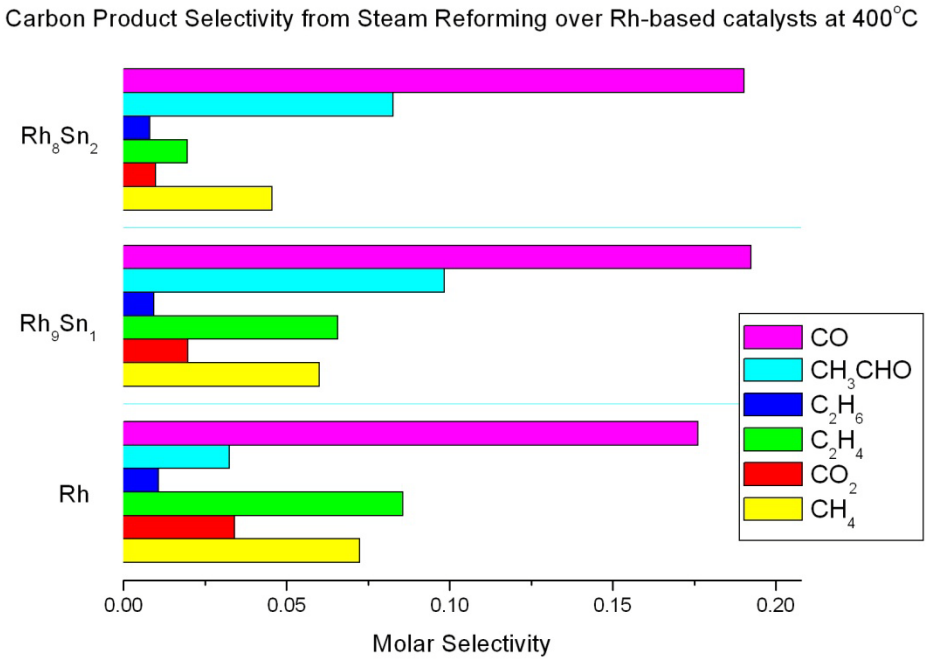

Figure 8: Plot of carbon product selectivity from steam reforming over Rh/CeO_2-based catalysts

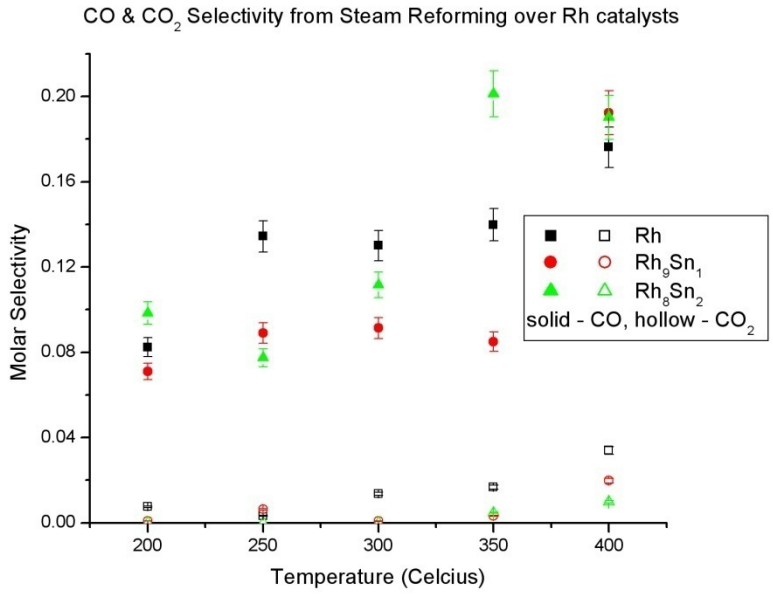

Figure 9: Plot of carbon monoxide and carbon dioxide selectivity from steam reforming over Rh/CeO_2-based catalysts

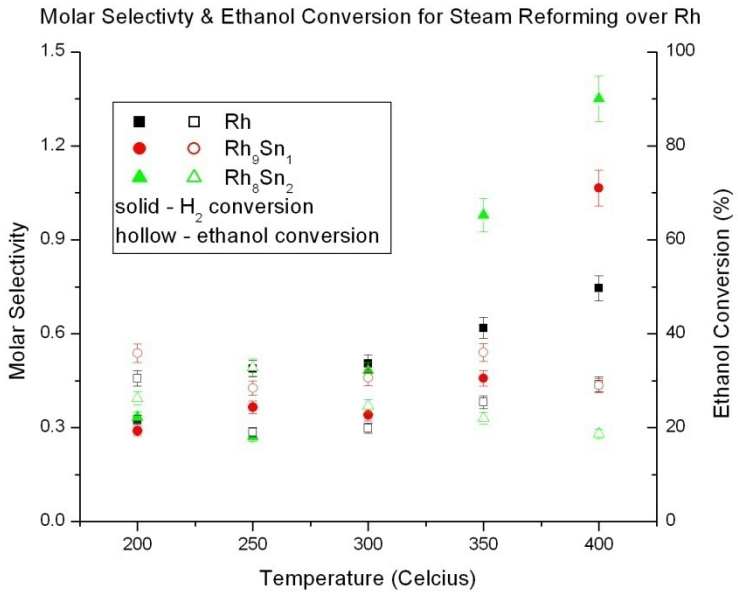

Figure 10: Plot of hydrogen selectivity and ethanol conversion from steam reforming over Rh/CeO_2-based catalysts

3.1.2 Pt_xSn_{1-x}/CeO_2, (x = 1, 0.9, 0.8)

Results for ethanol reforming over Pt-based catalysts are presented in Figures 11–16. The conversion of ethanol varied slightly between values of 25% and 40%, with no strong correlation to temperature for any of the catalysts. Selectivities for carbon dioxide and hydrocarbon production over Pt are similar to those over Rh; remaining small (≤ 0.1) and showing increases with increasing temperature. As shown in Figure 14, hydrocarbon and carbon dioxide selectivity was highest over the Pt_8Sn_2; while decreasing as Sn content in the catalyst decreases. Hydrogen selectivity and temperature dependent trends varied significantly as Sn content was added to the Pt catalyst. As temperature increased, molar selectivity to hydrogen increased over Pt and Pt_8Sn_2. Over the Pt_9Sn_1 catalyst, molar selectivity to hydrogen decreased slightly with increasing temperature from a value of 0.75 to 0.6. The selectivity to hydrogen at 200°C for the Pt_9Sn_1 catalyst was significantly larger than the other Pt catalyst systems studied. Above 250°C, hydrogen selectivity was slightly higher over the Pt_8Sn_2 system. Trends in carbon monoxide

selectivity for the different Pt-based systems approximately mirrored the hydrogen selectivity trends. Finally, selectivity to undetected carbon-containing products decreased as temperature increased and as the Sn composition of the catalyst increased. Given that this trend holds true for both Pt-based and Rh-based catalysts, these results suggest that the larger unidentified products play a significant role in ethanol reforming within this temperature range.

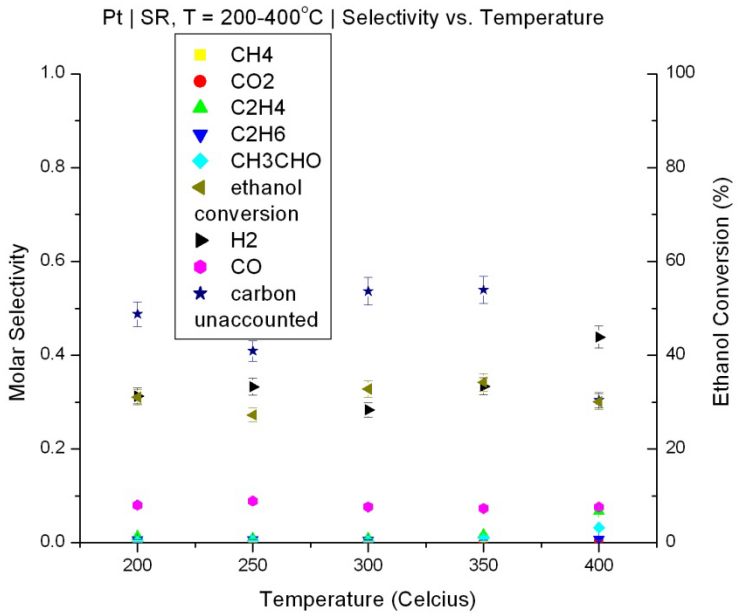

Figure 11: Plot of molar selectivity and ethanol conversion versus temperature over Pt/CeO_2 from steam reforming

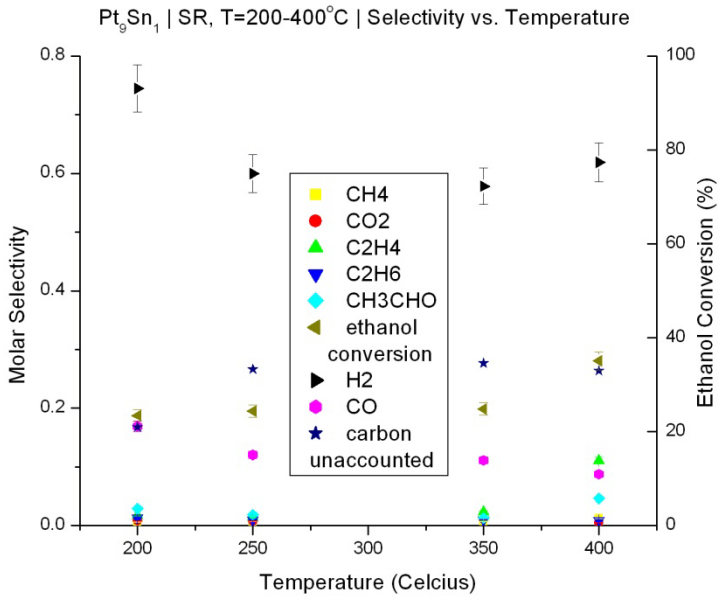

Figure 12: Plot of molar selectivity and ethanol conversion versus temperature over Pt_9Sn_1/CeO_2 from steam reforming

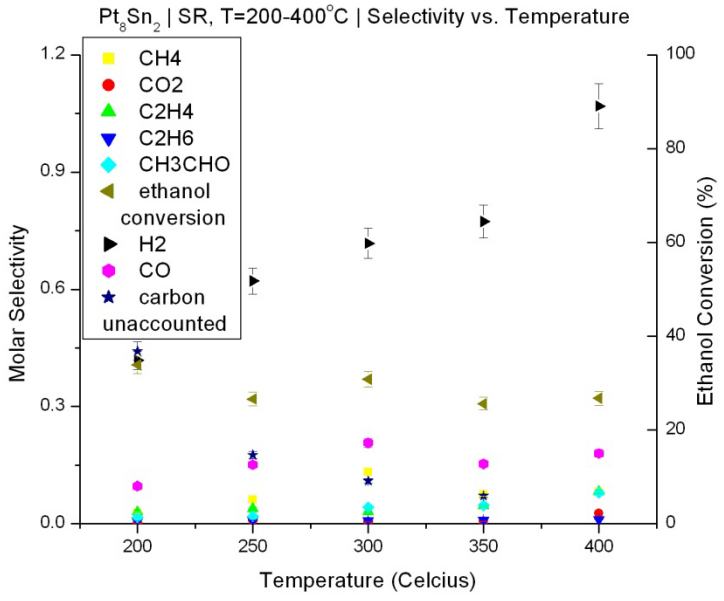

Figure 13: Plot of molar selectivity and ethanol conversion versus temperature over Pt_8Sn_2/CeO_2 from steam reforming

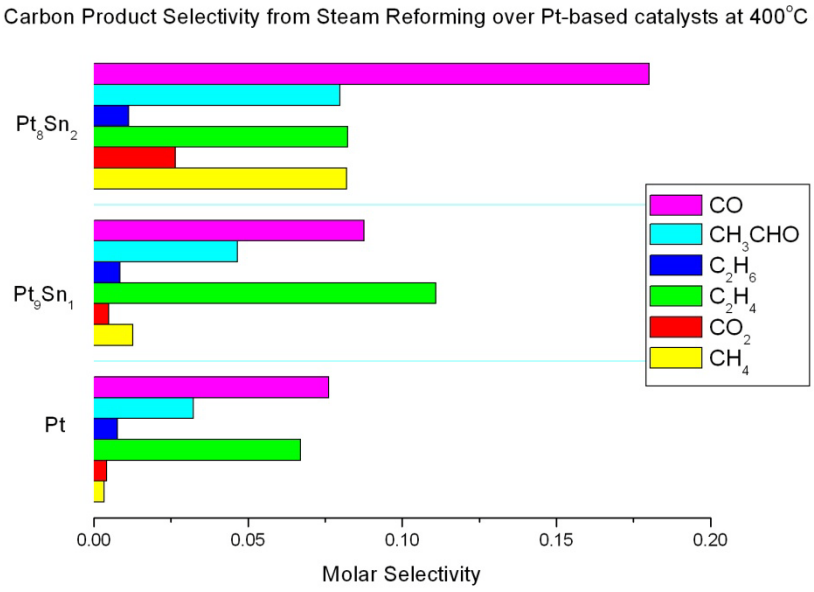

Figure 14: Plot of carbon selectivity from steam reforming over Pt/CeO_2-based catalysts from steam reforming

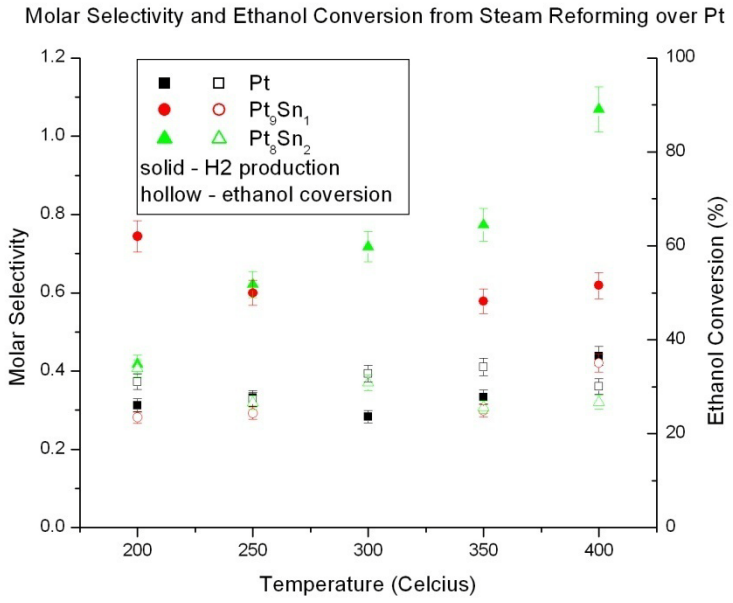

Figure 15: Plot of hydrogen selectivity and ethanol conversion from steam reforming over Pt/CeO_2-based catalysts

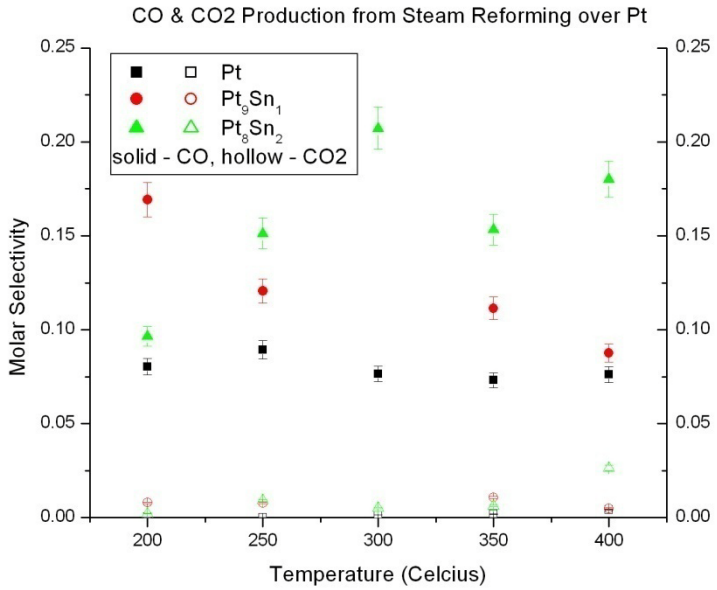

Figure 16: Plot of carbon monoxide and carbon dioxide selectivity from steam reforming over Pt/CeO_2-based catalysts

3.1.3 Activation Energies for Rate-Determining Reactions

Ethanol reforming over various catalyst systems was measured at various temperatures, in order to gain information about the reaction rate. Activation energies for the different byproduct species were derived from mathematical fitting to the Arrhenius relation

$$k = k^o \cdot exp\left[\frac{E_a}{R \cdot T}\right],$$

in which k is the rate constant, k^o is a constant pre-exponential factor, E_a is the activation energy of the rate-determining reaction step, R is the universal gas constant, and T is the absolute temperature. The production of byproducts measured at the outlet of the reactor was taken as the rate constant. Using the expression above, activation energies were derived from the steam reforming results shown in the Appendix. In Table 2, activation energies from steam reforming studies of various catalyst systems are displayed for byproducts with deterministic trends. Ethanol conversion to hydrogen was the most efficient over the Rh_8Sn_2 catalyst, followed by

Pt_8Sn_2, Rh, and Pt catalyst systems. The Rh and Rh_8Sn_2 catalyst produced carbon monoxide and some hydrocarbons with similar activation energies, while steam reforming over Rh_9Sn_1 and Pt_9Sn_1 is significantly less efficient for the same byproducts.

Table 2: Activation energies (kJ) for steam reforming byproducts detected between temperatures of 200°C and 400°C. (Activation energies calculated between temperatures of 200°C and 350°C)* (Activation energies calculated between temperatures of 300°C and 400°C)**

Catalyst	CH_4	CO_2	C_2H_4	C_2H_6	CH_3CHO	H_2	CO
5 % Rh / CeO_2	33	46	53	132	16	47	61
5 % Rh_9Sn_1 / CeO_2	49	104	90	113	73	66	104
5 % Rh_8Sn_2 / CeO_2*	75		45	54	45	82	120
5% Pt / CeO_2		17	89		52	50	
5% Pt_9Sn_1 / CeO_2	87		96	87		116	
5% Pt_8Sn_2 / CeO_2			112	68	17	51**	50**

When comparing the results of ethanol steam reforming over Rh-based catalyst systems studied, Rh_8Sn_2 showed the highest molar selectivity to hydrogen at 400°C and the highest activation energy for H_2. As indicated by the Arhenius Equation, a high activation energy correlates with strong temperature dependence; and Sn composition in the Rh catalysts strengthens this correlation in almost linear fashion. However, steam reforming over Pt-based catalyst systems showed less consistency in their species production trends or activation energies. Steam reforming over Pt_9Sn_1, produced the highest activation energy for hydrogen production amongst the Pt-based catalysts. Additionally, the high hydrogen selectivity at 200°C and the trend of decreasing hydrogen selectivity with increasing temperature over the Pt_9Sn_1 catalyst was an intriguing anomaly within this study. While the role of catalyst composition,

alloy microstructure, and reactor temperature may have varying or interrelated roles on byproduct selectivity; this result suggests that ethanol catalyst composition may be optimized for prime ethanol conversion within a range of temperatures. In addition, the trends presented suggest that there are several competing reaction pathways for hydrogen production within the temperature range studied. Carbon dioxide and carbon monoxide production over Pt catalysts was enhanced by the addition of a Sn component. On the other hand, carbon dioxide production over Rh catalysts systems was reduced by the presence of the Sn component. Additionally, the Pt-Sn catalyst systems were more effective in the production of hydrogen at low temperatures then were the Rh-Sn catalyst systems.

3.2 Oxidative Steam Reforming

In this study, oxidative steam reforming considers ethanol reforming in the presence of oxygen and steam in which Water:Ethanol:Oxygen = 1.8:1:0.6.

3.2.1 Rh_xSn_{1-x}/CeO_2, (x = 1, 0.9, 0.8)

Figures 17–21 show molar selectivity data plotted versus temperature over Rh-based catalysts. Compared to the steam reforming data, ethanol conversion in oxidative steam reforming is enhanced (40–60% for Rh-based catalysts). However, this enhancement leads to an increased selectivity of small carbon-containing species (CO, CO_2, and CH_4) and does not lead to an increased production or selectivity to hydrogen. Over the Rh catalyst, the molar selectivity to hydrogen was similar to the selectivity of methane and carbon monoxide (≈ 0.15), while carbon dioxide was produced at slightly larger selectivities. This trend remains fairly temperature independent below 350°C. Plots for oxidative steam reforming over Rh_9Sn_1 and Rh_8Sn_2 catalysts show similar trends in product selectivity. Selectivity to hydrogen, carbon monoxide, carbon dioxide, and methane was measured between 0.15 and 0.35 at temperatures of 350°C and below. Over the Rh_9Sn_1 catalyst, carbon dioxide decreased slightly and hydrogen increased

steadily with increasing temperature. Over Rh_8Sn_2, the selectivity of carbon dioxide peaked at 400°C, whereas selectivity to hydrogen and carbon monoxide decreased with increasing temperature. Selectivity to other detected byproducts (larger hydrocarbons) remained minimal (< 0.1) in all studies of oxidative steam reforming over Rh based samples. Selectivity to undetected carbon-containing products is shown in Figure 17, but was minimal over the remaining Rh-Sn systems.

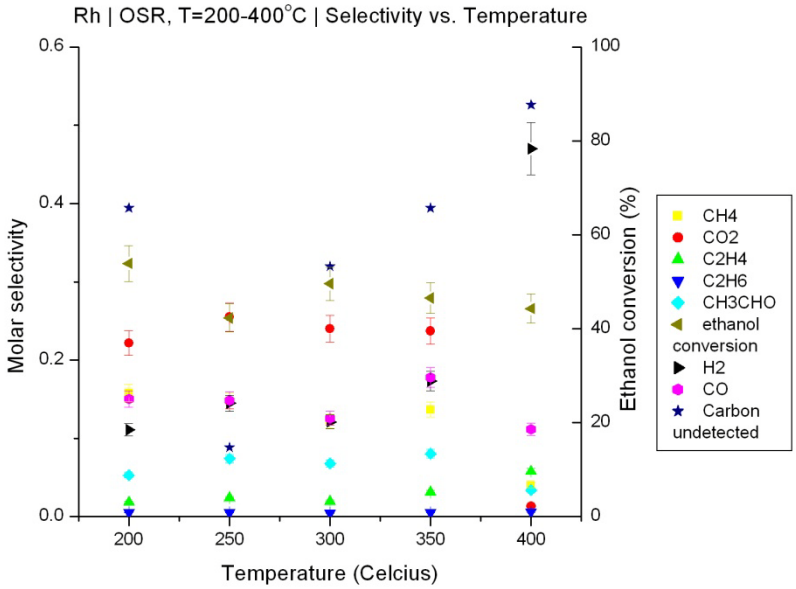

Figure 17: Plot of molar selectivity and ethanol conversion versus temperature over Rh/CeO_2 from steam reforming

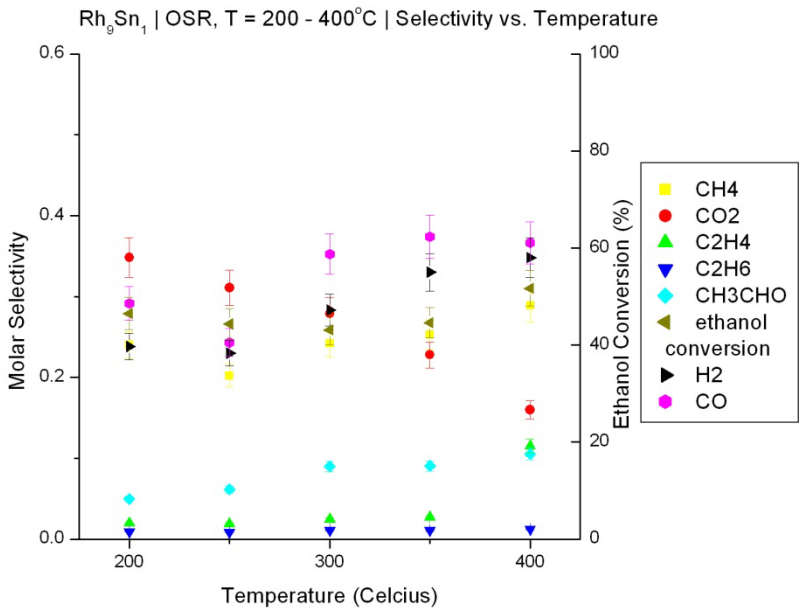

Figure 18: Plot of molar selectivity and ethanol conversion versus temperature over Rh_9Sn_1/CeO_2 from steam reforming

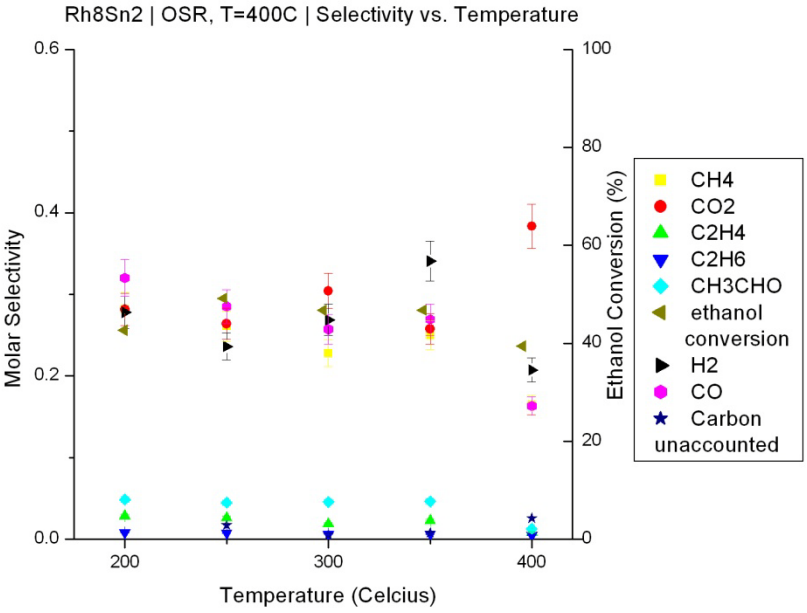

Figure 19: Plot of molar selectivity and ethanol conversion versus temperature over Rh_8Sn_2/CeO_2 from steam reforming

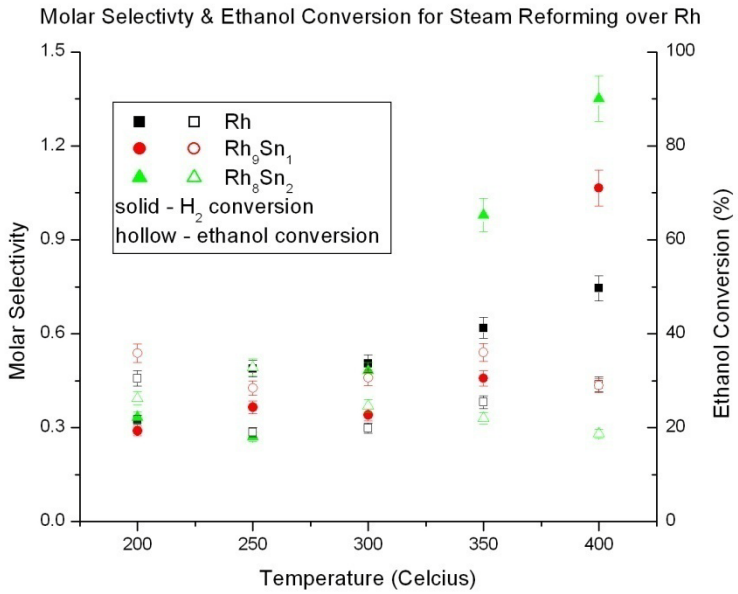

Figure 20: Plot of hydrogen selectivity and ethanol conversion over Rh/CeO_2-based catalysts from oxidative steam reforming

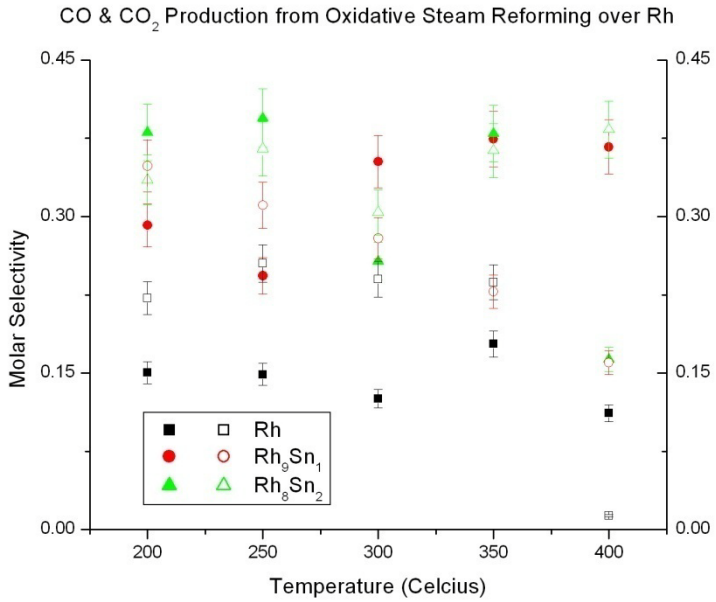

Figure 21: Plot of carbon monoxide and carbon dioxide selectivity over Rh/CeO_2-based catalysts from oxidative steam reforming

3.2.2 Pt_xSn_{1-x}/CeO_2, (x = 1, 0.9, 0.8)

Oxidative steam reforming results from Pt-based catalysts are presented in Figures 22-26. Ethanol conversion varied slightly with respect to temperature and was highest over the Pt_8Sn_2 catalyst (≈ 55%), followed by Pt_9Sn_1 (≈ 50%), and Pt (≈ 45%). These results show that increasing Sn content correlates directly to an increased ethanol conversion. As shown in Figures 25 & 26, increasing Sn content strongly correlated to increasing hydrogen selectivity, increasing carbon monoxide selectivity, and decreasing carbon dioxide selectivity. Hydrogen and carbon monoxide selectivities were highest over the Pt_8Sn_2 catalyst, followed by Pt_9Sn_1, and Pt. On average across the temperatures studied, carbon dioxide selectivity (0.15-0.35) was highest over the Pt catalysts, followed by Pt_9Sn_1, and Pt_8Sn_2 catalysts. Selectivity to hydrocarbons remained minimal (< 0.1) but was largest over Pt_8Sn_2. There were no strong temperature dependent trends observed.

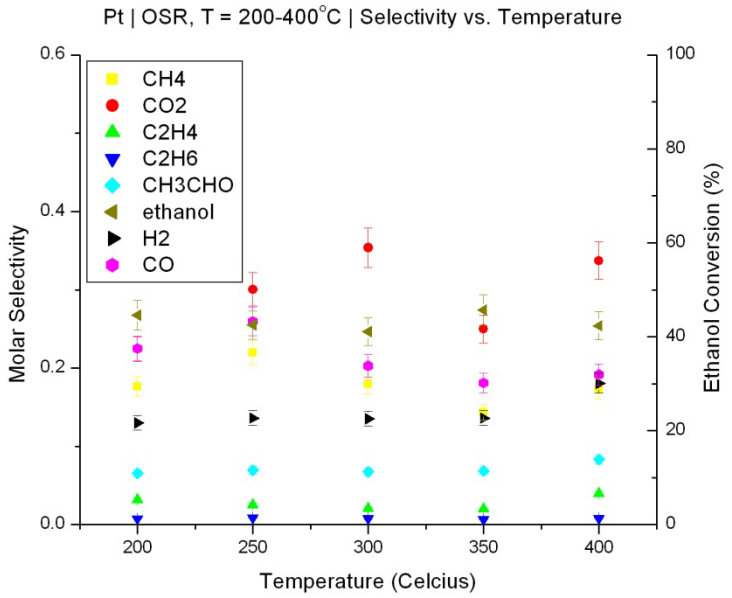

Figure 22: Plot of molar selectivity and ethanol conversion versus temperature over Pt/CeO_2 from oxidative steam reforming

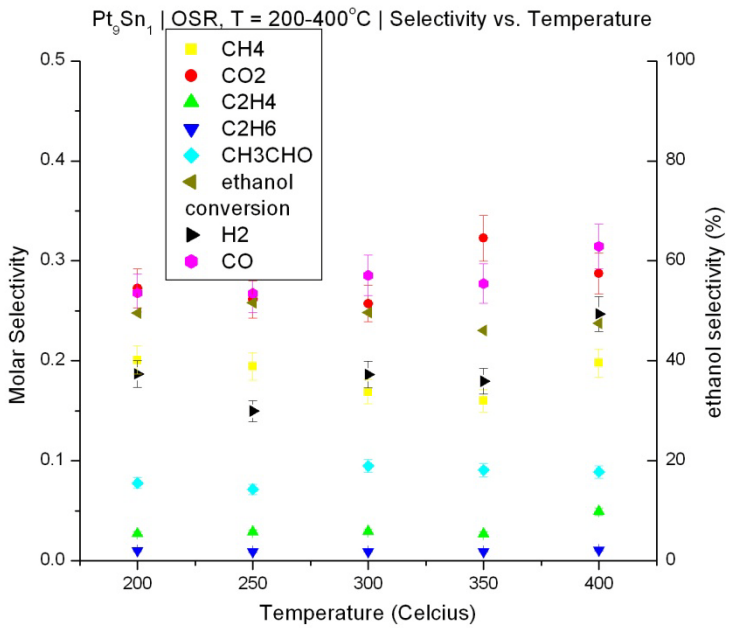

Figure 23: Plot of molar selectivity and ethanol conversion versus temperature from over Pt_9Sn_1/CeO_2 from oxidative steam reforming

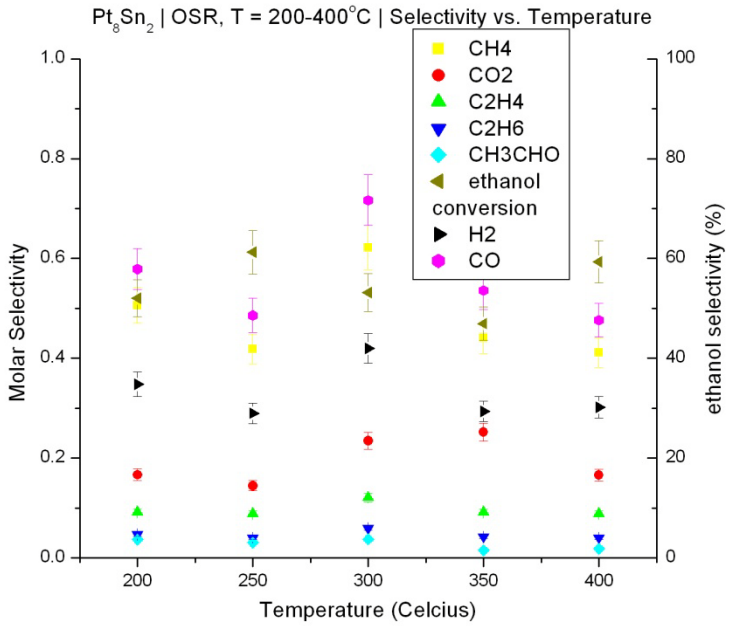

Figure 24: Plot of molar selectivity and ethanol conversion versus temperature over Pt_8Sn_2/CeO_2 from oxidative steam reforming

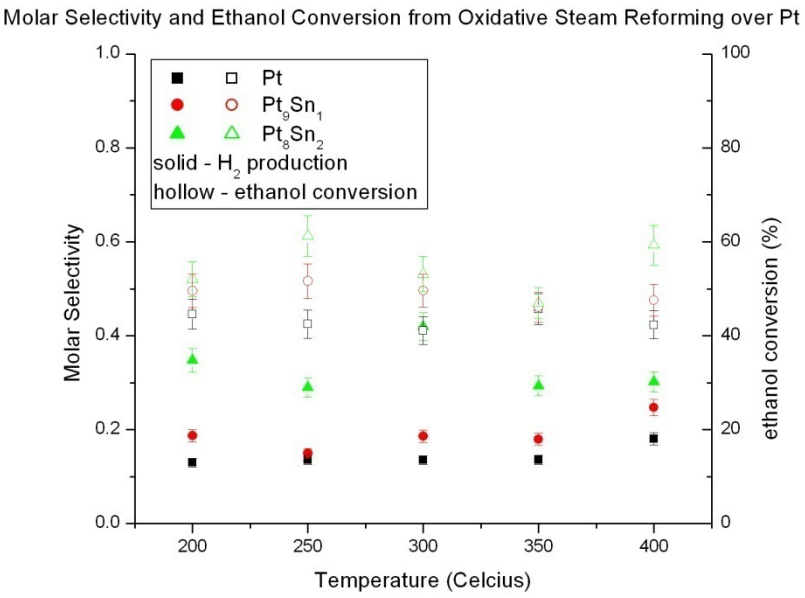

Figure 25: Plot of hydrogen selectivity and ethanol conversion over Pt/CeO_2-based catalysts from oxidative steam reforming

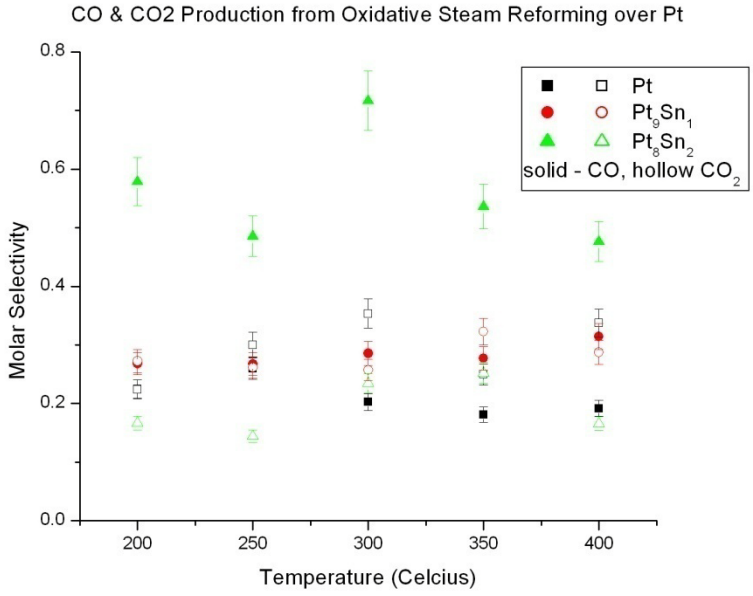

Figure 26: Plot of carbon monoxide and carbon dioxide selectivity over Pt/CeO_2-based catalysts from oxidative steam reforming.

Selectivities to products for oxidative steam reforming were significantly more independent of temperature than were byproduct selectivities from steam reforming. Additionally, the enhanced ethanol conversion improved production of carbon monoxide, carbon dioxide, and methane. However, hydrogen production was severely decreased and rendered oxidative steam reforming inefficient as compared to steam reforming. For these reasons, activation energies were not calculated for oxidative steam reforming products. Finally, the role of Sn on product selectivity and ethanol is more deterministic in conjunction with the Pt catalyst then with the Rh catalyst.

3.3 Ethanol Reforming with Varying Reactant Composition

Reforming products were additionally studied to determine the effect of shifts in reactant composition on the composition of product gas. The composition for one component of the reactant mixture was varied, while the other reactant components were held constant. Temperatures were held constant at 400°C. By varying reactant composition around the stoichiometric reactant ratios for steam reforming and oxidative steam reforming; and measuring the related changes in effluent production, we can calculate the reaction orders of the detected byproducts with respect to the variable reactant. In chemical kinetics, a reaction order with respect to a certain reactant is defined as the power to which a reactant's concentration affects the product's reaction rate. This relationship is expressed as

$$r = k[A]^x,$$

in which r is the reaction rate, k is the reaction constant, A is the reactant concentration, and x is the reaction order. Reaction order would be equal to the stoichiometric coefficient in a single-step elementary reaction. Using the expression above, byproduct reaction orders were derived from the steam reforming results shown in the Appendix. In this study, we will analyze reaction

orders for different byproducts and compare how reaction orders change with the catalyst compositions considered. This approach will allow us to identify which reactant components and catalyst compositions most strongly effect product composition.

Reaction orders for different steam reforming byproducts are shown in Tables 3–4. Information on the reactant compositions that produced the reaction orders is given in the subsequent tables. Reaction order information is most relevant for the largest products of steam reforming—hydrogen and carbon monoxide. Table 3 displays reaction orders for steam reforming byproducts in which the steam content was varied. It was unexpected that increasing steam content would slightly inhibit the production of H_2 for the case of steam reforming over Rh and Pt_8Sn_2; as hydrogen reaction orders would be positive based on reactions (1) and (2) . However, this is not the case for the remaining catalyst systems. Hydrogen production increased as steam concentration increased over Rh_9Sn_1, Rh_8Sn_2, Pt, and Pt_9Sn_1 catalyst systems. Due to similarities in the reaction orders for H_2 and CH_3CHO for the Rh-Sn catalysts systems, it is plausible that these species could be principally produced by ethanol dehydrogenation (11); which would corroborate these species' close reaction orders. Increasing water content in the reactant composition improved the production of carbon dioxide and methane over Rh_9Sn_1 and Pt_9Sn_1; while reducing production of these byproducts over Rh_8Sn_2 and Pt_8Sn_2. The role of increasing ethanol concentration on steam reforming over Rh catalyst improved the production of all identifiable products rather uniformly, and may be due to ethanol decomposition reactions (8-9) . Hydrogen and hydrocarbon production was enhanced more strongly by the ethanol concentration than by the water concentration when steam reforming is conducted over Rh & Pt catalyst systems; while hydrogen production is more effectively enhanced by water concentration over the Rh-Sn and Pt_9Sn_1 catalyst systems.

Table 3: Reaction orders of byproducts with respect to water for steam reforming over different catalysts. The ratio of water-to-ethanol in the reactant is 4.0–2.0. The ethanol flow rate is 10.4 sccm.

	CH_4	CO_2	C_2H_4	C_2H_6	CH_3CHO	H_2	CO
Rh	-0.334	0.772	-0.906	-0.031	-0.667	-0.211	-0.225
Rh_9Sn_1	0.789	0.695	-0.931	-0.938	0.955	0.858	0.924
Rh_8Sn_2	-0.073	-0.953	-0.709	0.932	0.955	0.964	-0.968
Pt	-0.169	-0.254	-0.994	-0.724	0.794	0.220	-0.656
Pt_9Sn_1	0.692	0.171	-0.2945	-0.811	.910	0.608	-0.179
Pt_8Sn_2	-0.555	-0.256	-0.9765	-1.000	-0.424	-0.578	0.896

Table 4: Reaction orders of byproducts with respect to ethanol for steam reforming over different catalysts. The ratio of water-to-ethanol in the reactant is 4.50–2.25. The water flow rate is 31.1 sccm.

	CH_4	CO_2	C_2H_4	C_2H_6	CH_3CHO	H_2	CO
Rh	0.768	0.792	0.889	0.713	0.893	0.83	0.754
Rh_9Sn_1	0.948	0.667	0.409	0.563	0.52	0.81	0.592
Rh_8Sn_2	0.669	-0.755	0.999	0.563	0.52	0.808	0.648
Pt	0.979	0.880	0.949	0.963	0.103	0.997	-0.997
Pt_9Sn_1	-0.362	-0.346	-0.094	-0.663	0.106	0.316	0.753
Pt_8Sn_2	-0.822	-0.353	0.863	-0.283	-0.227	-0.262	-0.941

Reaction orders for oxidative steam reforming byproducts are shown in Tables 5–6. Information on the reactant compositions that produced the reaction orders is given in the subsequent tables. Increasing steam concentration in the reactant composition has varying effects on hydrogen production. As shown in Table 5, hydrogen production decreased over Rh and Pt_9Sn_1;

while increasing over Rh_9Sn_1, Pt, and Pt_8Sn_2. On the other hand, increasing steam concentration favorably affected carbon monoxide and methane production over Rh, while decreasing carbon monoxide and methane production over Rh_9Sn_1, Pt, and Pt_9Sn_1. Increasing water concentration had less of an effect on production of these species over Rh_8Sn_2. Carbon dioxide production was enhanced by increasing water concentration in the reactant mixture over Rh and Pt. This trend was reversed over Pt-Sn systems and Rh_8Sn_2, as carbon dioxide production decreased with increasing steam concentration. In general, increasing water concentration in the reactant composition was more favorable to the production of carbon-containing species over Rh and Pt while promoting hydrogen production over Rh_9Sn_1 and Pt_8Sn_2 catalyst systems. In Table 6, reaction orders with respect to oxygen were shown for various byproducts. Increasing the oxygen content of the reactants lead to increases in hydrogen production over Rh and decreases in hydrogen production over the Rh-Sn and Pt-based catalyst systems. The primary effect of increasing the oxygen reactant composition was an almost linear increase in the production of carbon dioxide for all catalyst systems studied; and the order of the carbon dioxide reaction is strongly corroborated by the species order in stoichiometric partial oxidation reaction (4) and the stoichiometric oxidative steam reforming reaction (7). Methane production increased with increasing oxygen reactant composition, but this effect decreased as Sn was added to the catalyst composition. Additionally, increasing oxygen content in the reactant composition lead to increased carbon monoxide production over Rh and Rh_8Sn_2, while decreasing carbon monoxide production over Rh_9Sn_1 and Pt-based catalyst systems.

Table 5: Reaction order of byproducts with respect to water for oxidative steam reforming over different catalysts. The ratio of water-to-ethanol is 2.4–1.2. The ethanol flow rate is 15.7 sccm and the oxygen rate is 9.4 sccm.

	CH_4	CO_2	C_2H_4	C_2H_6	CH_3CHO	H_2	CO
Rh	0.932	0.784	0.431	0.984	0.825	-0.611	0.863
Rh_9Sn_1	-0.877	0.295	-0.088	-0.987	-0.858	0.706	-0.91
Rh_8Sn_2	-0.194	-0.797	0.436	0.362	0.995	0.042	0.149
Pt	-0.670	1.000	0.183	-0.780	0.270	0.407	-0.836
Pt_9Sn_1	-0.999	-0.988	-0.664	-0.995	0.042	-0.861	-1
Pt_8Sn_2	-0.332	-0.976	0.362	0.133	0.159	0.499	.207

Table 6: Reaction order of byproducts with respect to oxygen for oxidative steam reforming over different catalysts. The ratio of oxygen-to-ethanol is 0.4–0.8. The water flow rate is 28.2 sccm and the oxygen 9.4 sccm.

	CH_4	CO_2	C_2H_4	C_2H_6	CH_3CHO	H_2	CO
Rh	0.902	0.913	0.681	0.854	1	0.822	-0.422
Rh_9Sn_1	0.709	0.926	-0.104	0.883	-0.401	-0.455	0.833
Rh_8Sn_2	0.246	1.000	-0.965	0.384		-0.995	-0.909
Pt	0.997	1.000	-0.685	0.993	0.016	-0.604	0.992
Pt_9Sn_1	0.905	0.973	0.692	0.912	0.991	-0.190	0.980
Pt_8Sn_2	0.443	0.972	-0.319	0.206	-0.645	-0.471	0.409

As shown in Table 7, increasing ethanol content in the reactant composition lead to various effects on the reaction order of byproducts over the catalysts studied. Hydrogen production over Rh and Rh_9Sn_1 and Pt_8Sn catalysts was improved by increasing ethanol content, while hydrogen production was reduced by increasing ethanol composition over Pt_9Sn_1 catalysts.

Also, hydrocarbon byproducts were predominantly decreased over Rh and Rh_8Sn_2, while increasing over Rh_9Sn_1 and Pt-based catalysts.

Table 7: Reaction order of byproducts with respect to ethanol for oxidative steam reforming over different catalysts. The ratio of water-to-ethanol is 2.70–1.35. The water flow rate is 28.2 sccm and the oxygen 9.4 sccm.

	CH_4	CO_2	C_2H_4	C_2H_6	CH_3CHO	H_2	CO
Rh	-0.937	-0.915	-0.918	-0.988	-1	0.844	-0.952
Rh_9Sn_1	0.88	0.821	0.278	0.572	0.472	0.98	-0.794
Rh_8Sn_2	-0.493	0.741	-0.513	-0.377	-0.656	-0.507	-0.331
Pt	0.171	-0.576	0.974	-0.017	0.439	0.518	0.424
Pt_9Sn_1	0.793	-0.949	0.829	-0.286	0.996	-0.933	-0.430
Pt_8Sn_2	0.876	-0.933	0.935	0.763	0.960	0.967	0.860

Based on this analysis, ethanol reforming over Pt, Pt_8Sn, and Rh_9Sn_1 is favored using a reactant mixture composed primarily of steam and ethanol as opposed to oxidative steam reforming conditions. Ethanol reforming over Pt_9Sn_1 would benefit from a reactant composition rich in oxygen and ethanol.

4 Conclusion and Future Work

Binary metallic catalysts offer several advantages over single-phase metal catalysts for the purposes of low-temperature ethanol reforming. Steam reforming over Pt-Sn and Rh-Sn catalysts showed improvements in hydrogen selectivity over single-phase Pt and Rh catalysts between 200°C and 400°C. Ethanol reforming over Pt_8Sn_2 and Rh_8Sn_2 offered lower activation energies for hydrogen then single-phase systems offered; and thus the most efficient of the systems considered for the production of hydrogen. However, ethanol reforming over Pt_9Sn_1 and Rh_9Sn_1 yielded activation energies for hydrogen that were higher than the single-phase systems. The most surprising result was that the Pt_9Sn_1 catalyst system showed the largest hydrogen selectivity and productivity at 200°C of all the catalyst systems considered. These results demonstrate the plausibility of catalytic ethanol reforming in a temperature range that would be suitable for the operation of solid acid fuel cells and polymer electrolyte membrane fuel cells. Selectivity trends and kinetic information suggest that the role of catalyst composition may have a primary but varying role on the ethanol reforming reaction mechanism. Additionally, it was unexpected that increasing steam content would slightly inhibit the production of hydrogen over Rh and Pt_8Sn_2. However, steam reforming over the Rh-Sn and Pt_9Sn_1 catalyst systems favors a reactant mixture with a rich steam composition.

Oxidative steam reforming over these catalyst systems showed improvements in ethanol conversion, and production of carbon monoxide, carbon dioxide, and methane. However, hydrogen production was severely decreased, and renders oxidative steam reforming inefficient as compared to steam reforming. By calculating the yield of undetected carbon-containing products and showing how production of carbon-containing products decreases with increasing temperature, this study indicates the need for a more complete identification of ethanol reforming byproducts at low temperature. The ability to identify all reforming byproducts

would further clarify selectivity trends, kinetic reaction parameters, and possible reaction mechanism.

This study has served to elucidate the relationship between ethanol reforming conditions, catalyst composition, and resultant product composition in a temperature that has been frequently disregarded by similar studies of ethanol conversion. Kinetic parameters have been identified and certain trends in product selectivity have been highlighted; but there is much work to be done before establishing a credible model of the ethanol reforming reaction mechanism or optimizing a catalyst for ethanol reforming.

Amongst the catalyst systems considered for ethanol steam reforming, hydrogen production was highest over Pt_9Sn_1 and Rh_8Sn_2 for the temperature range of 200^{o}C to 400^{o}C. Further hydrogen production and kinetic information could be obtained from decreasing the reactant's flow rate and increasing the reactant's steam content during reforming over these catalyst systems. The resulting conditions would serve to enhance hydrogen production and ethanol conversion, while providing more kinetic information from which to assess the associated reaction mechanism.

A similar study of different Pt-Rh-Sn catalyst systems would be useful in clarifying how catalyst composition effects ethanol reforming. Previous studies of ternary catalyst systems have suggested that synergistic interactions between catalyst components can allow new reaction pathways for ethanol reforming. Given that in this study, hydrogen selectivity peaks at different temperatures for Pt_9Sn_1 and Pt_8Sn_2, ethanol reforming over an optimized Pt-Rh-Sn catalyst system could reveal more information about the role of catalyst composition and reactor temperature.

Finally, additional experimental methods could be used to analyze reforming byproducts and to further characterize the catalyst materials employed. The use of a GC/MS would extend analysis

of ethanol conversion by detecting liquid products—particularly some heavier carbon-containing compounds. A complete picture of reforming byproducts could help to identify possible reaction pathways, as well as address other issues of catalyst deactivation and optimal reactor conditions.

5 Acknowledgements

This work has been funded by The James Irvine Foundation and the California Institute of Technology, Office of Graduate Studies. Additional support has been provided by the Office of Naval Research and the Global Climate and Energy Program of Stanford University.

I'd like to sincerely thank my thesis committee—Dr. Sossina M. Haile, Dr. Kaushik Bhattacharya, and Dr. Joseph E. Shepherd. These scientists have offered their academic support and their patience. My deepest appreciation is offered to my advisor Sossina, whose bold scholarship and steadfast vision in her field have motivated me to push past earlier setbacks and to see this journey to its full completion. I've been profoundly humbled by the guidance of Dr. David Goodwin, whose sense of creativity and adventure first garnered my interest in the study of fuel cells and interfacial chemistry. This experience has been greatly strengthened by the collaborative efforts and the friendship of Dr. Adrian Hightower. The opportunity to complete this study would not have been possible without his inspiration and advocacy.

In addition, Professor Ken Pickar has my gratitude for allowing me the privilege to serve as his teaching assistant and—despite my naivety—the opportunity to take part in the rewriting of his course curriculum. The experience afforded me training and mentorship that has and continues to profoundly shape my aspirations as an educator. Thanks are due to my friends and colleagues for all the ways that they have contributed to my graduate education, for both challenging and championing my work, for their emotional support, and for their persistent motivation when I had little left and less to give in return. Continued love to my parents, Quida and Eugene. Thank you for nurturing me, for showing me how to love, and for teaching me what in life is worth the fight.

This thesis is dedicated to the memory of Elaine Joy Aton de la Cruz. I remain indebted to her friendship, her consciousness and the boldness with which she pursued her life.

All praise is due to the creator. Any errors, omissions, or oversimplifications are my own, for which I accept full responsibility and seek forgiveness.

6 References

1. O. Akdim, W. Cai, V. Fierro, H. Provendier, A. van Veen, W. Shen, and C. Mirodatos. Oxidative Steam Reforming of Ethanol over Ni–Cu/SiO_2, Rh/Al_2O_3 and Ir/CeO_2: Effect of Metal and Support on Reaction Mechanism. *Top Catal* 51 2008: 22–38.
2. F. Aupretre, C. Descorme, and D. Duprez. Hydrogen production for fuel cells from the catalytic ethanol steam reforming. *Top Catal* 30 2004: 487-491
3. F. Aupretre, C. Descorme, D. Duprez, D. Casanave, and D. Uzio. Ethanol steam reforming over $Mg_xNi_{1-x}Al_2O_3$ spinel oxide-supported Rh catalysts. *Journal of Catalysis*. 233 2005: 464-477.
4. P. Bera and J. M. Vohs. Reaction of CH_3OH on Pd/ZnO(0001) and PdZn/ZnO(0001) Model Catalysts. *J. Phys. Chem. C* 111 2007: 7049-7057.
5. J.L. Bi, Y.Y. Hong, C.C. Lee, C.T. Yeh, and C.B. Wang. Novel zirconia-supported catalysts for low-temperature oxidative steam reforming of ethanol. *Catalysis Today* 129 2007: 322–329.
6. F. Colmati, E. Antolini, E.R. Gonzalez. Preparation, structural characterization and activity for ethanol oxidation of carbon supported ternary Pt–Sn–Rh catalysts. *J. of Alloys and Compounds*: 456 2008: 264–270.
7. Y. Chen, Z. Shao, and N. Xu. Ethanol Steam Reforming over Pt Catalysts Supported on $Ce_xZr_{1-x}O_2$ Prepared via a Glycine Nitrate Process. *Energy & Fuels* 22 2008: 1873–1879.
8. S.M. de Lima, I.O. da Cruz, G. Jacobs, B.H. Davis, L.V. Mattos, and F.B. Noronha. Steam reforming, partial oxidation, and oxidative steam reforming of ethanol over Pt/$CeZrO_2$ catalyst. *Journal of Catalysis* 257 2008: 356–368.

9. J.P.I. de Souza, S.L. Queiroz, K. Bergamaski, E.R. Gonzalez, and F.C. Nart. Electro-Oxidation of Ethanol on Pt, Rh, and PtRh Electrodes. A Study Using DEMS and in-Situ FTIR Techniques. *J. Phys. Chem. B* 106 2002: 9825-9830
10. A. Erdohelyi, J. Raskó, T. Kecskés, M. Tóth, M. Dömök, and K. Baán. Hydrogen formation in ethanol reforming on supported noble metal catalysts. *Catalysis Today* 116 2006: 367–376.
11. A.E. Farrell, R.J. Plevin, B.T. Turner, A.D. Jones, M. O'Hare, and D.M. Kammen. Ethanol Can Contribute to Energy and Environmental Goals. *Science*. 311 27 January 2006: 506-508.
12. F. Frusteri, S. Freni, L. Spadaro, V. Chiodo, G. Bonura, S. Donato, and S. Cavallaro. H_2 production for MC fuel cell by steam reforming of ethanol over MgO supported Pd, Rh, Ni and Co catalysts. *Catalysis Communications* 5 2004: 611–615.
13. A. Haryanto, S. Fernando, N. Murali, and S.l. Adhikari. Current Status of Hydrogen Production Techniques by Steam Reforming of Ethanol: A Review. *Energy & Fuels*. 19 2005: 2098-2106.
14. H. Idriss, C. Diagne, J. P. Hindermann, A. Kiennemann, and M.A. Barteau. Reactions of Acetaldehyde on CeO_2 and CeO_2-Supported Catalysts. *Journal of Catalysis* 155 1995: 219-237.
15. G. Jacobs, R.A. Keogh, and B.H. Davis. Steam reforming of ethanol over Pt/ceria with co-fed hydrogen. *Journal of Catalysis* 245 2007: 326–337.
16. L. Jiang, G. Sun, S. Sun, J. Liu, S. Tang, H. Li, B. Zhou, and Q. Xin. Structure and chemical composition of supported Pt–Sn electrocatalysts for ethanol oxidation. *Electrochimica Acta* 50 2005: 5384–5389.

17. A. Kowal, S.Lj. Gojkovic, K.S. Lee, P. Olszewski, and Y.E. Sung. Synthesis, characterization and electrocatalytic activity for ethanol oxidation of carbon supported Pt, Pt–Rh, Pt–SnO_2 and Pt–Rh–SnO_2 nanoclusters. *Electrochemistry Communications* 11 2009: 724–727
18. F.H.B. Lima and E.R. Gonzalez. Ethanol electro-oxidation on carbon-supported Pt–Ru, Pt–Rh and Pt–Ru–Rh nanoparticles. *Electrochimica Acta* 53 2008: 2963–2971.
19. S.S.Y. Lin, D.H. Kim, and S.Y. Ha. Hydrogen Production from Ethanol Steam Reforming Over Supported Cobalt Catalysts. *Catal Lett* 122 2008: 295–301.
20. L.V. Mattos and F.B. Noronha. Partial oxidation of ethanol on supported Pt catalysts. *Journal of Power Sources* 145 2005: 10–15.
21. L.V. Mattos and F.B. Noronha. The influence of the nature of the metal on the performance of cerium oxide supported catalysts in the partial oxidation of ethanol. *Journal of Power Sources* 152 2005: 50–59.
22. M. Mavrikakis, D.J. Doren, and M.A. Barteau. Density Functional Theory Calculations for Simple Oxametallacycles: Trends across the Periodic Table. *Journal of Physical Chemistry B* 102 1998: 394-399.
23. K.D. Pointon. Review of work on internal reforming in the Solid Oxide Fuel Cell. British Gas plc. *Crown*. 1997.
24. J. Raskó, A. Hancz, and A. Erdóhelyi. Surface species and gas phase products in steam reforming of ethanol on TiO_2 and Rh/TiO_2. *Applied Catalysis A: General* 269 2004: 13-25.
25. J. Ribeiro, D.M. dos Anjos, K.B. Kokoh , C. Coutanceau, J.M. Léger, P. Olivi, A.R. de Andrade, and G. Tremiliosi-Filho. Carbon-supported ternary PtSnIr catalysts for direct ethanol fuel cell. *Electrochimica Acta* 52 2007: 6997–7006.

26. J. Ribeiro, D.M. dos Anjos, J.M. Léger, F. Hahn, P. Olivi, A.R. de Andrade, G. Tremiliosi-Filho, and K.B. Kokoh. Effect of W on PtSn/C catalysts for ethanol electrooxidation. J. Appl. *Electrochem.* 38 2008: 653-662.

27. H.S. Roh, Y. Wang, D.L. King, A. Platon, and Y.H. Chin. Low temperature and H_2 selective catalysts for ethanol steam reforming. *Catalysis Letters* 108 2006: 15-19.

28. P.Y. Sheng, A.Yee, G.A. Bowmaker, and H. Idriss. H_2 Production from Ethanol over Rh–Pt/CeO2 Catalysts: The Role of Rh for the Efficient Dissociation of the Carbon–Carbon Bond. *Journal of Catalysis*. 208 2002: 393-403.

29. M. Singh, N. Zhou, D.K. Paul, and K.J. Klabunde. IR spectral evidence of aldol condensation: Acetaldehyde adsorption over TiO_2 surface. *Journal of Catalysis* 260 2008: 371–379.

30. N. Srisiriwat, S. Therdthianwong, and A. Therdthianwong. Oxidative steam reforming of ethanol over Ni/Al_2O_3 catalysts promoted by CeO_2, ZrO_2 and CeO_2–ZrO_2. International Journal of Hydrogen Energy 34 2009: 2224-2234.

31. J. Sun, X.P. Qiu, F. Wu, W.T. Zhu. H_2 from steam reforming of ethanol at low temperature over Ni/Y_2O_3,Ni/La_2O_3 and Ni/Al_2O_3 catalysts for fuel-cell application. *International Journal of Hydrogen Energy* 30 2005: 437 – 445

32. A. Trovarelli. Catalytic properties of ceria and CeO_2-containing materials *Catalysis reviews: science and engineering*. 38 1996: 439-520.

33. P.D. Vaidya and A.E. Rodrigues. Insight into steam reforming of ethanol to produce hydrogen for fuel cells. *Chemical Engineering Journal*. 117 2006: 39-49.

34. F. Vigier, C. Coutanceau, F. Hahn, E.M. Belgsir, and C. Lamy. On the mechanism of ethanol electro-oxidation on Pt and PtSn catalysts: electrochemical and in situ IR reflectance spectroscopy studies. *Journal of Electroanalytical Chemistry* 563 2004: 81–89.
35. M. Watanabe and S. Motoo. Electrocatalysis by Ad-atoms. Part 1. Enhancement of oxidation of methanol on platinum and palladium by gold ad-atoms. *Journal of Electroanalytical Chemistry* 60 1976: 259-266.
36. M. Watanabe and S. Motoo. Electrocatalysis by Ad-atoms. Part 2. Enhancement of oxidation of methanol on platinum by ruthenium ad-atoms. *Journal of Electroanalytical Chemistry* 60 1976: 267-273.
37. M. Watanabe and S. Motoo. Electrocatalysis by Ad-atoms. Part 3. Enhancement of oxidation of carbon-monoxide on platinum by ruthenium ad-atoms. *Journal of Electroanalytical Chemistry* 60 1976: 275-283.
38. G. Wu, R. Swaidan, and G. Cui. Electrooxidations of ethanol, acetaldehyde and acetic acid using PtRuSn/C catalysts prepared by modified alcohol-reduction process. *Journal of Power Sources* 172 2007: 180–188.
39. A. Yee, S.J. Morrison, and H. Idriss. A Study of Ethanol Reactions over Pt/CeO_2 by Temperature-Programmed Desorption and in Situ FT-IR Spectroscopy: Evidence of Benzene Formation. *Journal of Catalysis* 191 2000: 30–45.
40. L. Zhang, J. Liu, W. Li, C. Guo, and J. Zhang. Ethanol steam reforming over Ni-Cu/Al2O3-M_yO_z (M = Si, La, Mg, and Zn) catalysts. *Journal of Natural Gas Chemistry* 18 2009: 55–65.

7 Appendix: Plots of Ethanol Reforming Byproducts for Catalysts Studied

The following plots derived from the study of ethanol reforming catalysts over Pt-based and Rh-based catalysts. 'Production v.s. Temperature' plots display measured resultant volumetric gas composition over a temperature range of 200°C to 400°C. 'Arhenius Plots' show the logarithm of volumetric gas composition versus the logarithm of the inverse absolute temperature (K^{-1}). We can use the relationship

$$k = y_o + Ae^{-E/RT},$$

to represent the production of ethanol reforming byproducts; in which k is the byproduct gas composition, T is absolute temperature in Kelvins, R is the gas constant, E is activation energy, A is the exponential prefactor. In this experiment, y_o corresponds to the ethanol conversion that occurs in the reactor without contact with the catalyst bed (i.e. thermodynamically, as a function of heating in the reactor prior to the reactant's contact with the catalyst bed). In the table below, the experimentally measured value of y_o (the steam reforming that occurs in the reactor at 200°C, without the presence of the catalyst bed) is compared to the numerical fit to y_o, as generated from the data in Figure 61 and 73. The close agreement between the experimental and numerically fit values in Table 8 shows that ethanol conversion prior to the reactor bed does contribute to the formation of ethanol reforming products at a consistent level.

Table 8: Conversion of ethanol in the reactor, outside of the catalyst bed.

y_o value for fitting of steam reforming data	Log (CH4)	Log (C2H4)	Log (H2)	Log (CH4)
Measured (Sand only/ catalyst removed, 200°C)	-2.40	-1.87	-0.20	-0.84
Fit from Steam Reforming over Pt_8Sn_2	-2.29	-1.85	-0.32	-0.84
Fit from Steam Reforming over Pt_9Sn_1	-2.23	-1.84	-0.25	-0.84

From the Arhenius plots, we may derive the activation energy for each product species we detect via numerical fitting. Finally, log-log plots display the logarithm of gas composition versus the logarithm of reactant composition. The linear slope of each byproduct's data set in these plots equates to the reaction orders for the production of the measured product species. The values derived from these plots are presented in the Results and Data Analysis Section of this paper.

7.1 Ethanol Reforming over Rh (5% wt.)/CeO_2

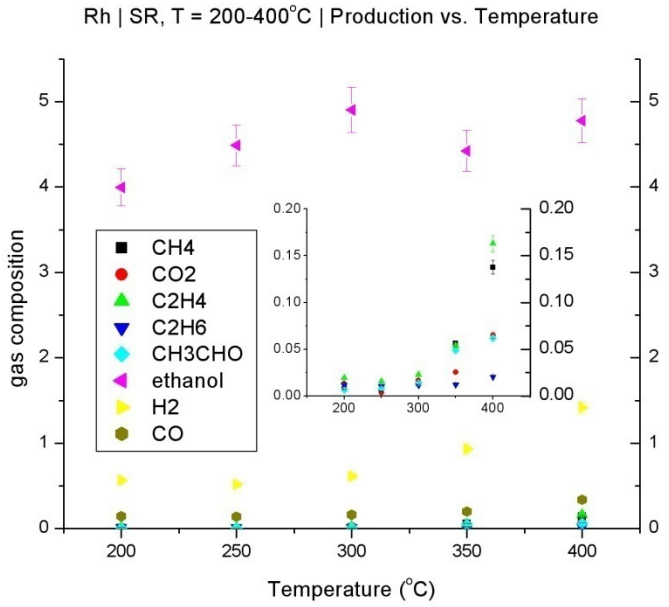

Figure 27: Product gas composition versus Temperature for steam reforming. Molar ratio of water-to-ethanol in the reactant gas is 3:1. The ratio of catalyst mass to reactant flow is 7.8 kg · sec /m, while ethanol vapor and steam flow rates were set at 10 and 31 sccm.

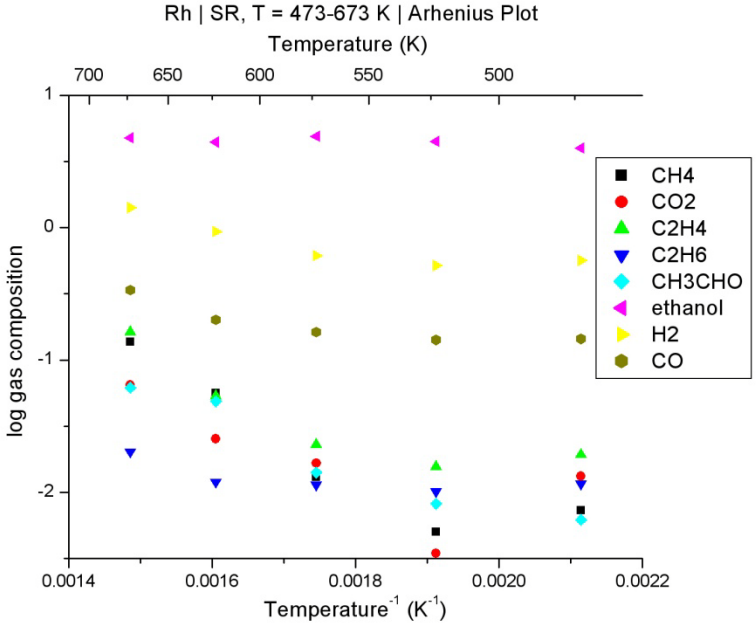

Figure 28: Arhenius plot of the product gas composition for steam reforming.

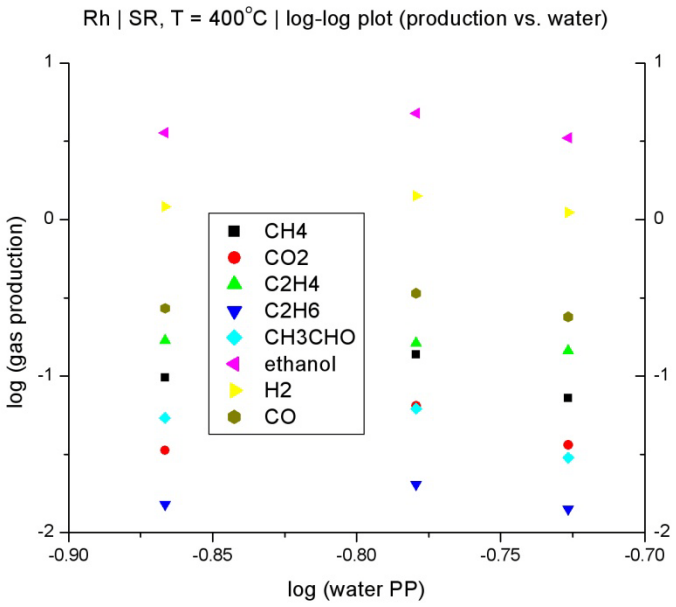

Figure 29: Log-log plot of product gas composition versus the inlet steam partial pressure. The ratio of catalyst mass to reactant flow was 6.2 – 10.4 kg · sec/m. Ethanol flow rate was held constant at 10.4 sccm.

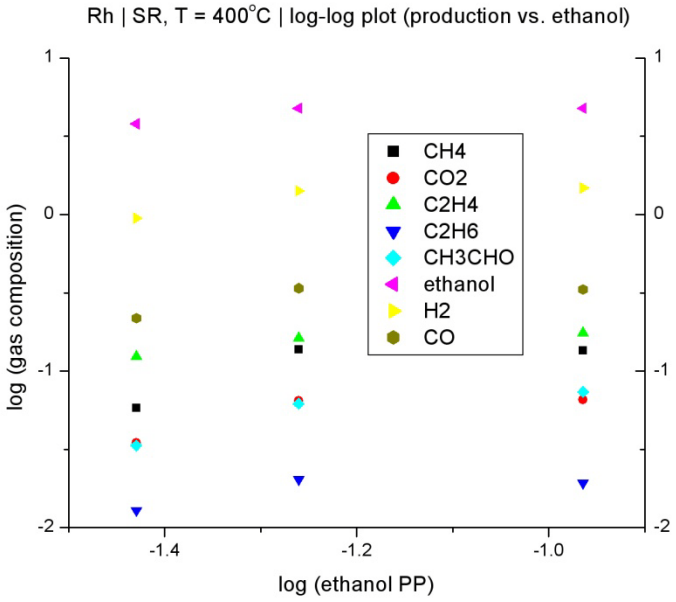

Figure 30: Log-log plot of product gas composition versus the inlet ethanol partial pressure. The ratio of catalyst mass to reactant flow was 7.2 – 8.5 kg · sec/m. Steam flow rate has held constant at 31.1 sccm.

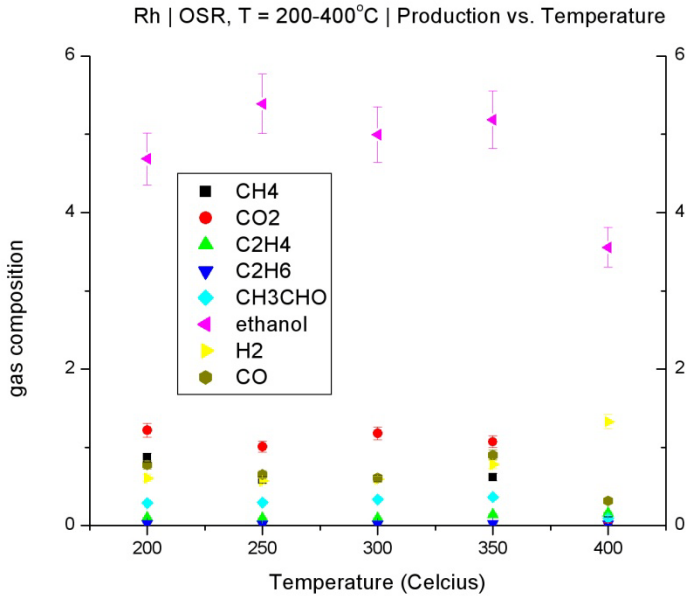

Figure 31: Product gas composition versus temperature for oxidative steam reforming. Molar ratio of water-to-ethanol-to-oxygen in the reactant gas is 1.8:1.0:0.6. The ratio of catalyst mass to reactant flow was 6.1 kg · sec/m, while ethanols vapor, steam, oxygen and argon flow rates were set to 15.7, 28.2, 9.4 and 120 sccm, respectively.

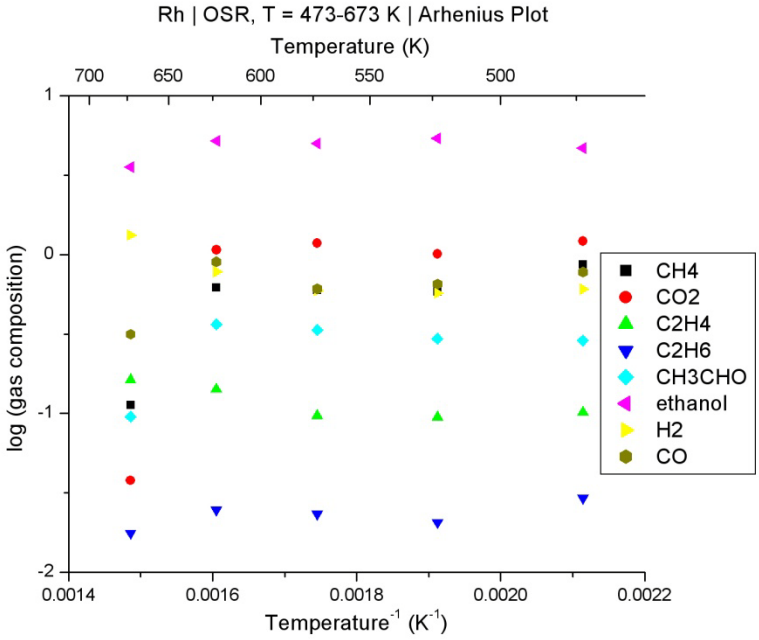

Figure 32: Arhenius plot of the product gas composition for oxidative steam reforming.

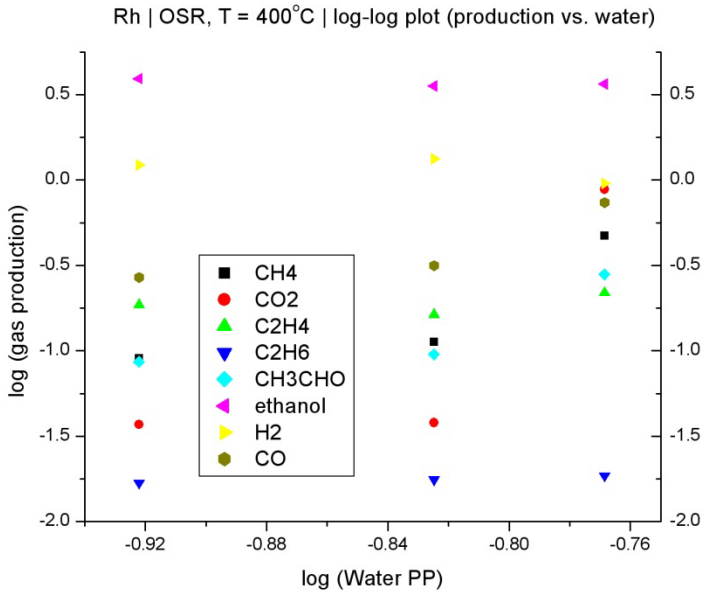

Figure 33: Log-log plot of product gas composition versus the inlet steam partial pressure. The ratio of catalyst mass to reactant flow was 5.2 – 7.4 kg · sec/m. Ethanol and oxygen flow rates were held constant at 9.4 and 15.7 sccm. The molar ratio of water:ethanol:oxygen in the reactant gas is 1.2-2.4:1:0.6.

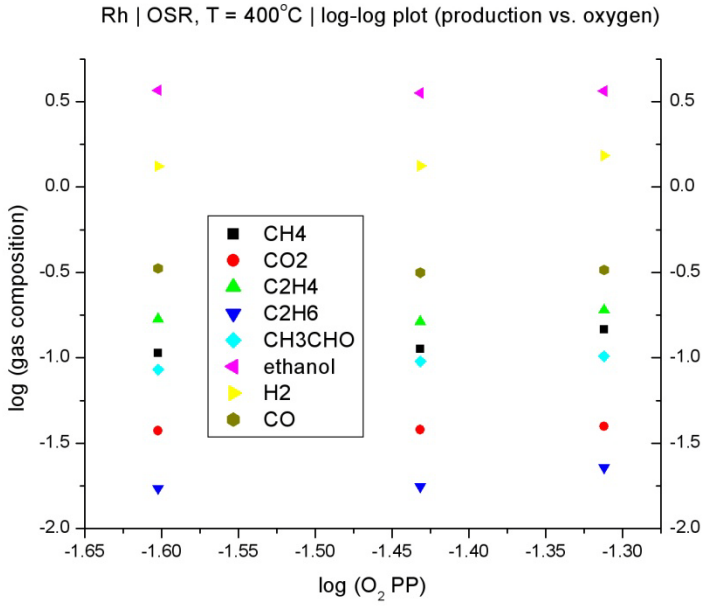

Figure 34: Log-log plot of product gas composition versus the inlet oxygen partial pressure. The ratio of catalyst mass to reactant flow was 5.7 – 6.3 kg · sec/m. Ethanol and steam flow rates were held constant at 15.7 and 28.2 sccm. The molar ratio of water:ethanol:oxygen in the reactant gas 1.8:1:0.4-0.8

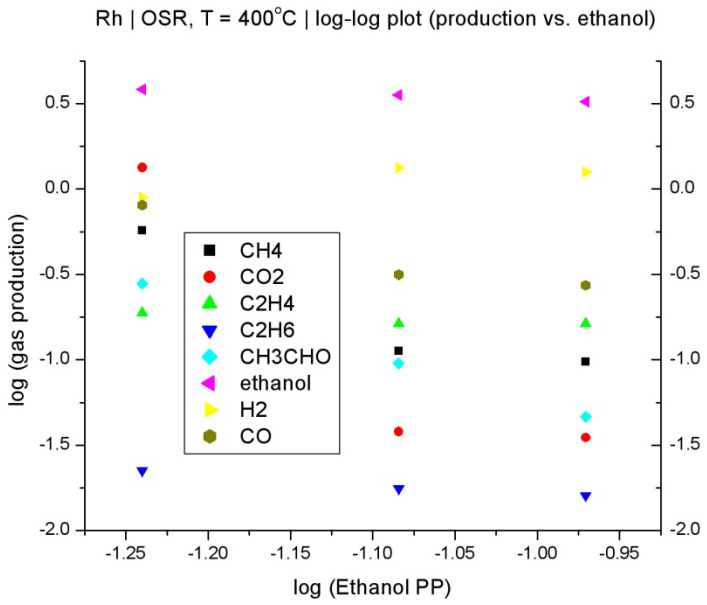

Figure 35: Log-log plot of product gas composition versus the inlet ethanol partial pressure. The ratio of catalyst mass to reactant flow was 5.5 – 6.7 kg · sec/m. Oxygen and steam flow rates were held constant at 9.4 and 28.2 sccm. The molar ratio of water:ethanol:oxygen in the reactant gas 1.8:1.33-0.66:0.6.

7.2 Ethanol Reforming over Rh_9Sn_1 (5% wt.)/CeO_2

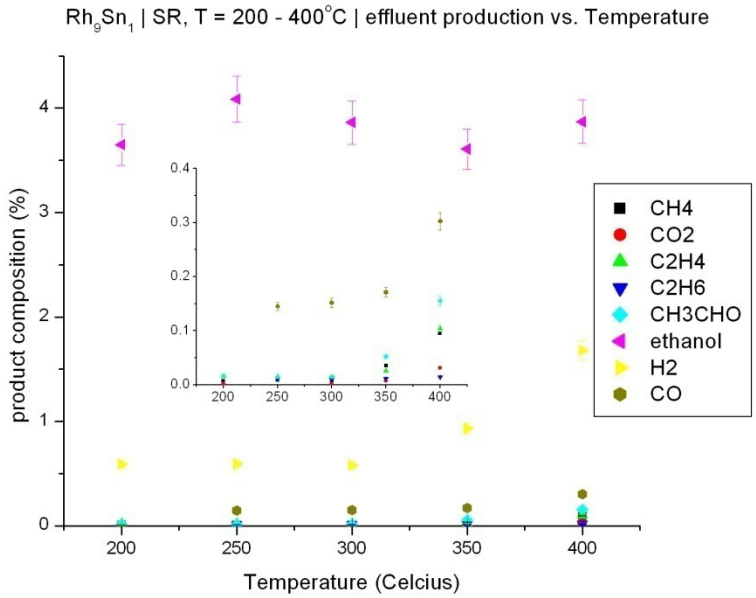

Figure 36: Product gas composition versus Temperature for steam reforming. Molar ratio of water-to-ethanol in the reactant gas is 3:1. The ratio of catalyst mass to reactant flow was 7.8 kg · sec/m, while ethanol vapor and steam flow rates were set at 10 and 31 sccm.

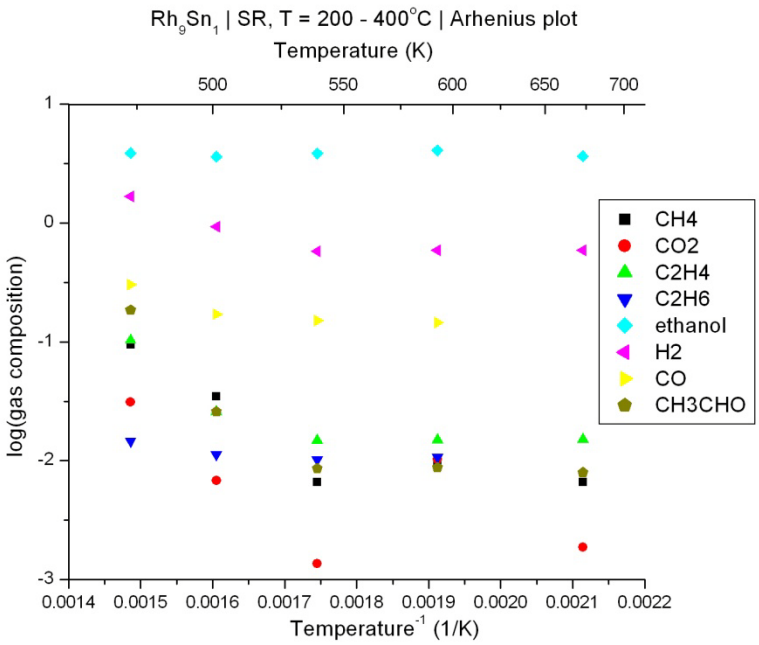

Figure 37: Arhenius plot of the product gas composition for steam reforming.

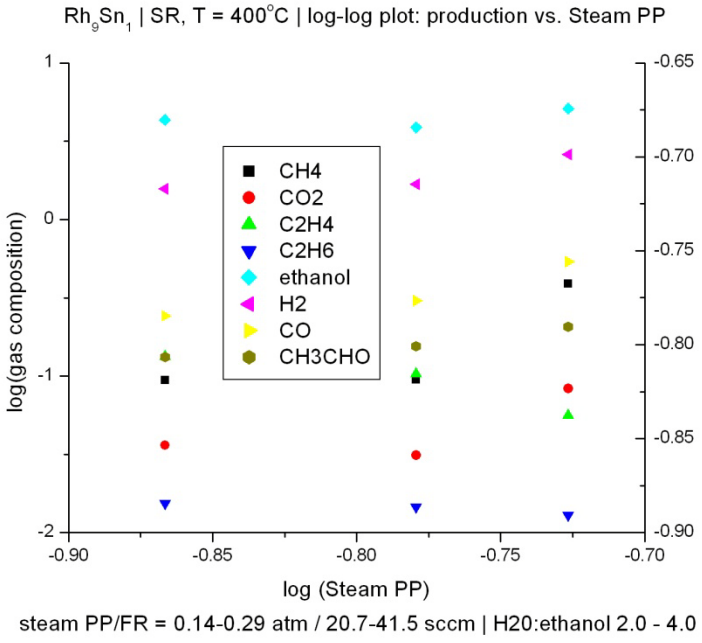

Figure 38: Log-log plot of product gas composition versus the inlet steam partial pressure. The ratio of catalyst mass to reactant flow was 6.2 – 10.4 kg · sec/m. Ethanol flow rate was held constant at 10.4 sccm.

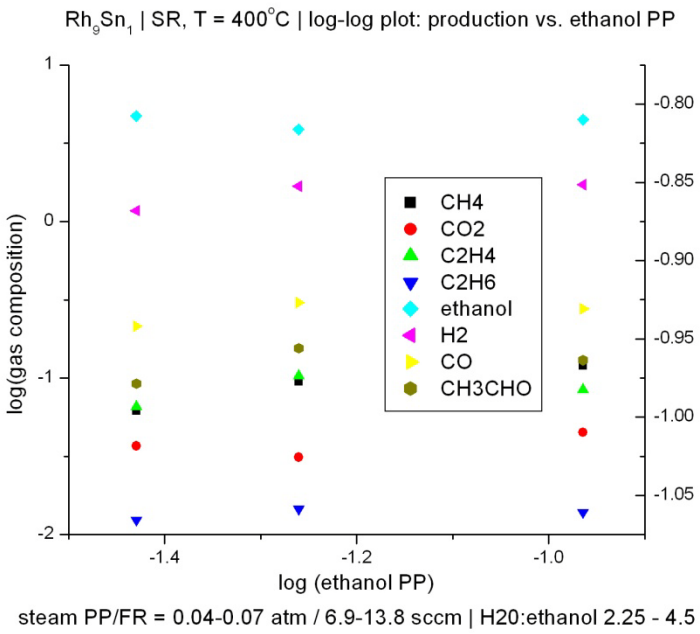

Figure 39: Log-log plot of product gas composition versus the inlet ethanol partial pressure. The ratio of catalyst mass to reactant flow was 7.2 – 8.5 kg · sec/m. Steam flow rate has held constant at 31.1 sccm.

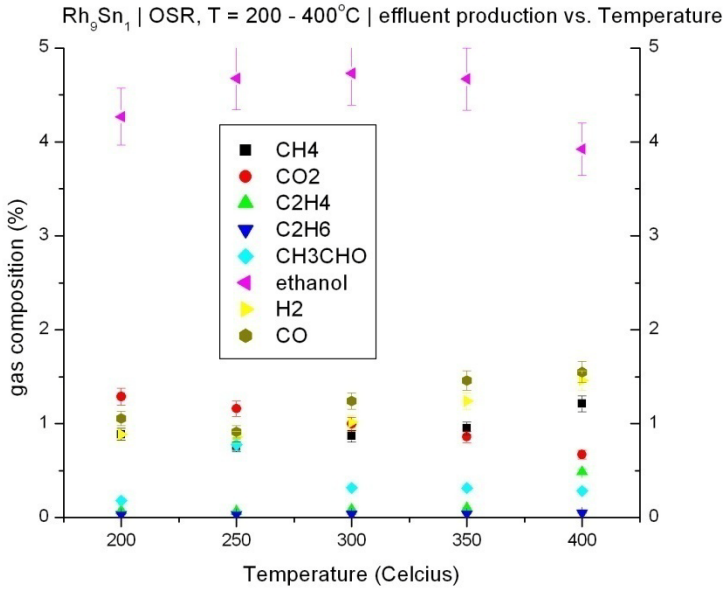

Figure 40: Product gas composition versus temperature for oxidative steam reforming. Molar ratio of water-to-ehanol-to-oxygen in the reactant gas is 1.8:1.0:0.6. The ratio of catalyst mass to reactant flow was 6.1 kg · sec/m, while ethanol vapor, steam, oxygen and argon flow rates were set to 15.7, 28.2, 9.4 and 120 sccm, respectively.

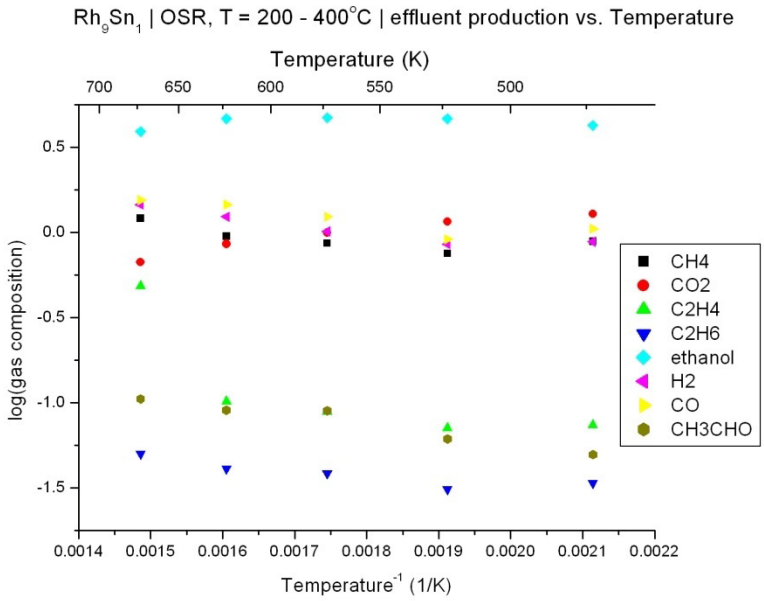

Figure 41: Arhenius plot of the product gas composition for oxidative steam reforming.

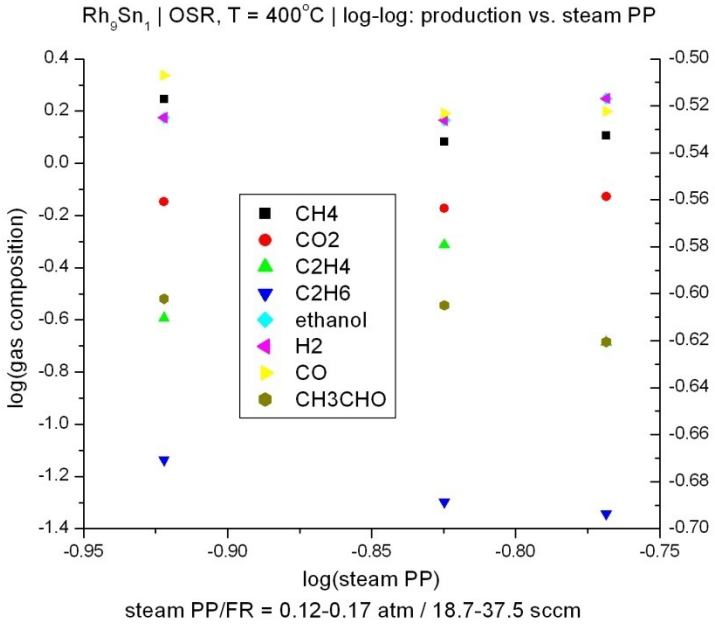

Figure 42: Log-log plot of product gas composition versus the inlet steam partial pressure. The ratio of catalyst mass to reactant flow was 5.2 – 7.4 kg · sec/m. Ethanol and oxygen flow rates were held constant at 9.4 and 15.7 sccm. The molar ratio of water:ethanol:oxygen in the reactant gas is 1.2-2.4:1:0.6.

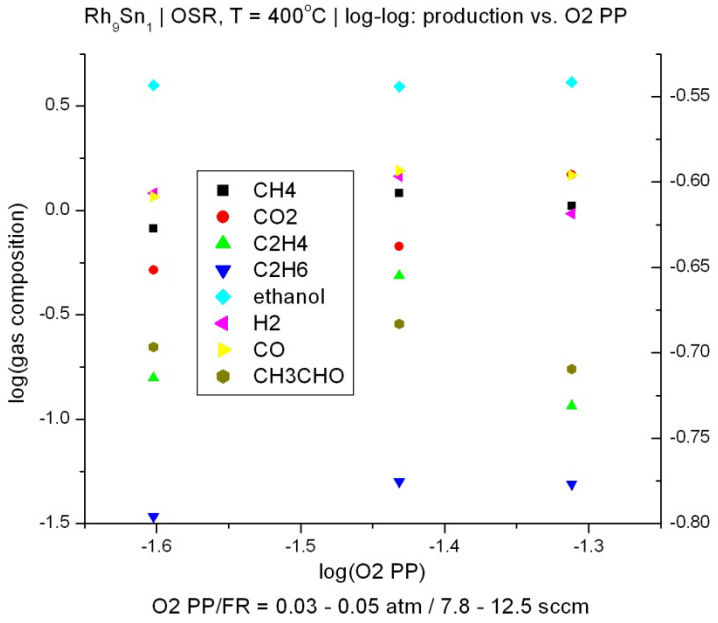

Figure 43: Log-log plot of product gas composition versus the inlet oxygen partial pressure. The ratio of catalyst mass to reactant flow was 5.7 – 6.3 kg · sec/m. Ethanol and steam flow rates were held constant at 15.7 and 28.2 sccm. The molar ratio of water:ethanol:oxygen in the reactant gas 1.8:1:0.4-0.8.

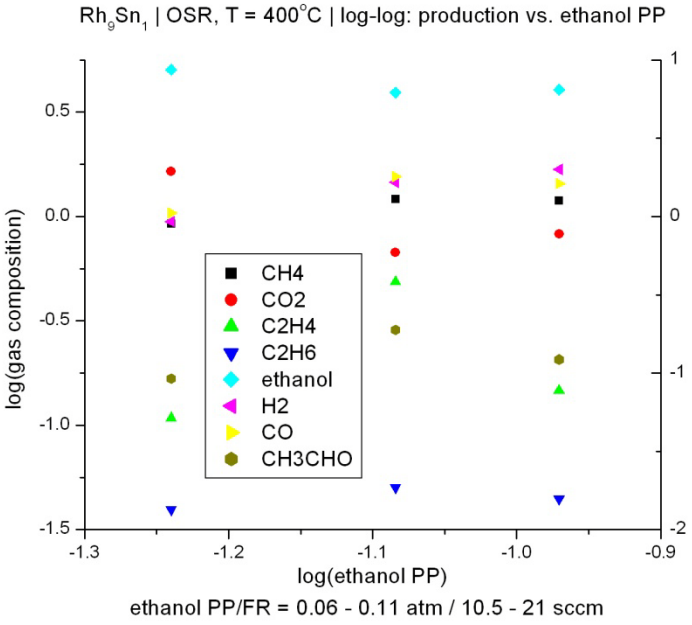

Figure 44: Log-log plot of product gas composition versus the inlet ethanol partial pressure. The ratio of catalyst mass to reactant flow was 5.5 – 6.7 kg · sec/m. Oxygen and steam flow rates were held constant at 9.4 and 28.2 sccm. The molar ratio of water:ethanol:oxygen in the reactant gas 1.8:1.33-0.66:0.6.

7.3 Ethanol Reforming over Rh_8Sn_2 (5% wt.)/CeO_2

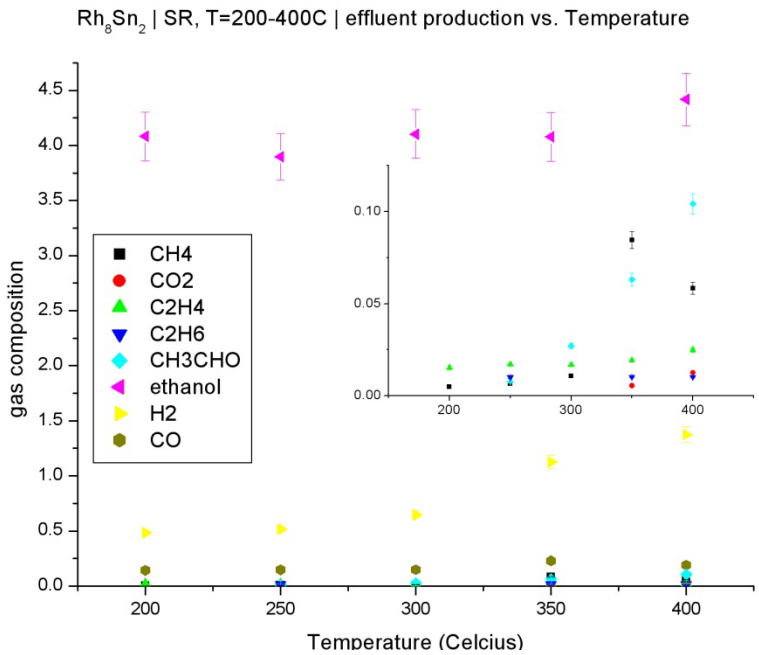

Figure 45: Product gas composition versus Temperature for steam reforming. Molar ratio of water-to-ethanol in the reactant gas is 3:1. The ratio of catalyst mass to reactant flow was 7.8 kg · sec /m, while ethanol vapor and steam flow rates were set at 10 and 31 sccm.

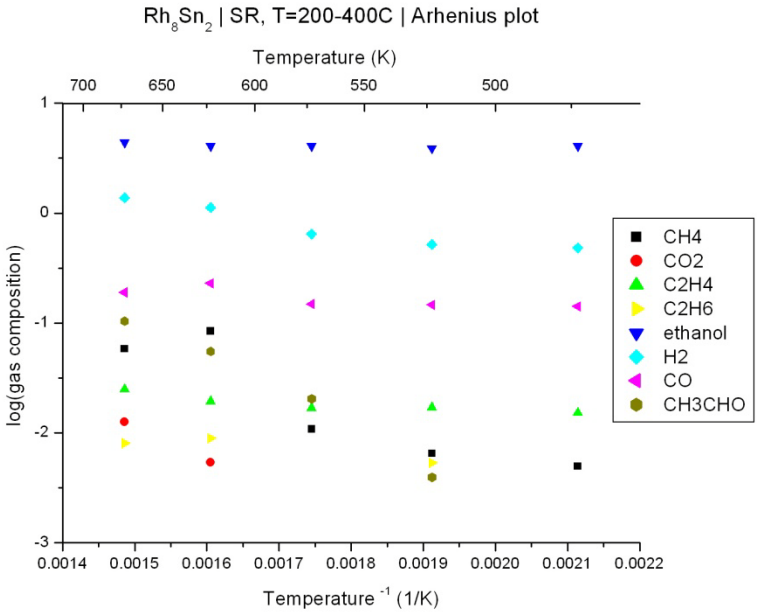

Figure 46: Arhenius plot of the product gas composition for steam reforming.

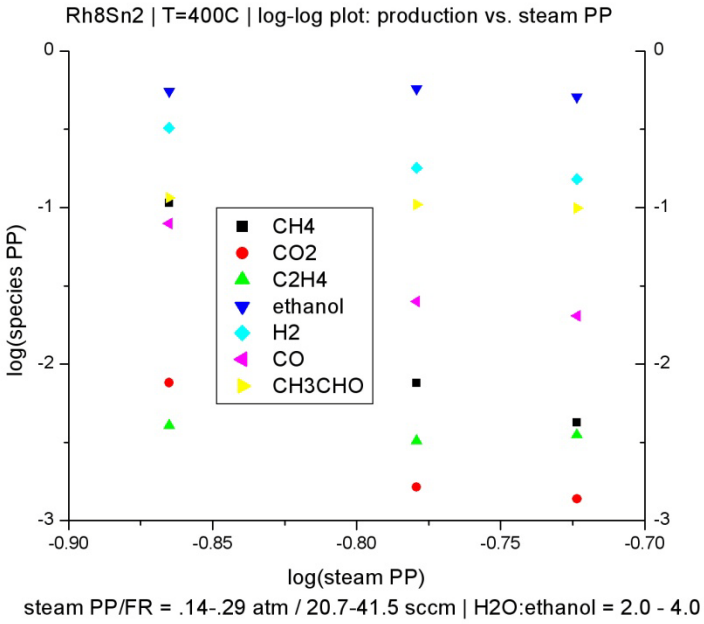

Figure 47: Log-log plot of product gas composition versus the inlet steam partial pressure. The ratio of catalyst mass to reactant flow was 6.2 – 10.4 kg · sec/m. Ethanol flow rate was held constant at 10.4 sccm.

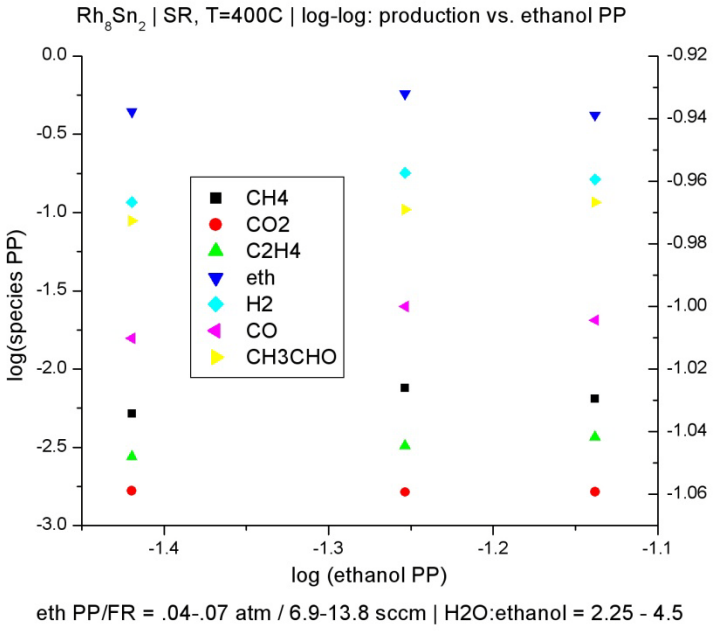

Figure 48: Log-log plot of product gas composition versus the inlet ethanol partial pressure. The ratio of catalyst mass to reactant flow was 7.2 – 8.5 kg · sec/m. Steam flow rate has held constant at 31.1 sccm.

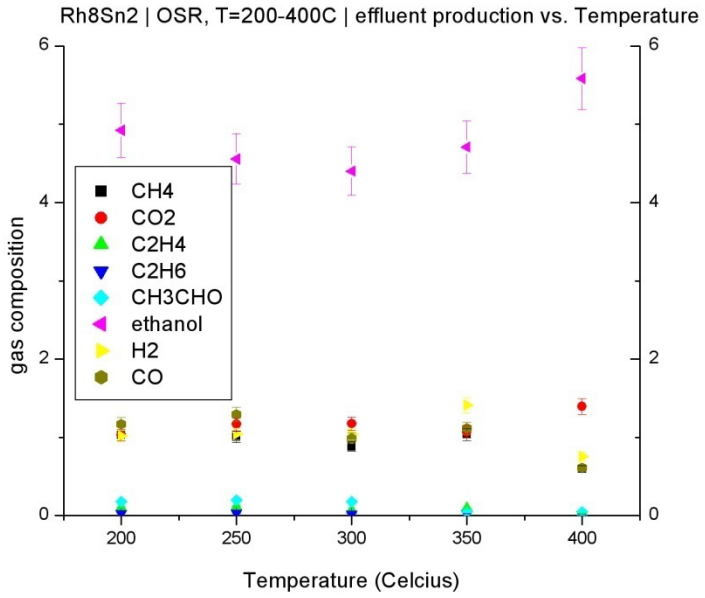

Figure 49: Product gas composition versus temperature for oxidative steam reforming. Molar ratio of water-to-ethanol-to-oxygen in the reactant gas is 1.8:1.0:0.6. The ratio of catalyst mass to reactant flow was 6.1 kg · sec/m was used, while ethanol vapor, steam, oxygen and argon flow rates were set to 15.7, 28.2, 9.4 and 120 sccm, respectively.

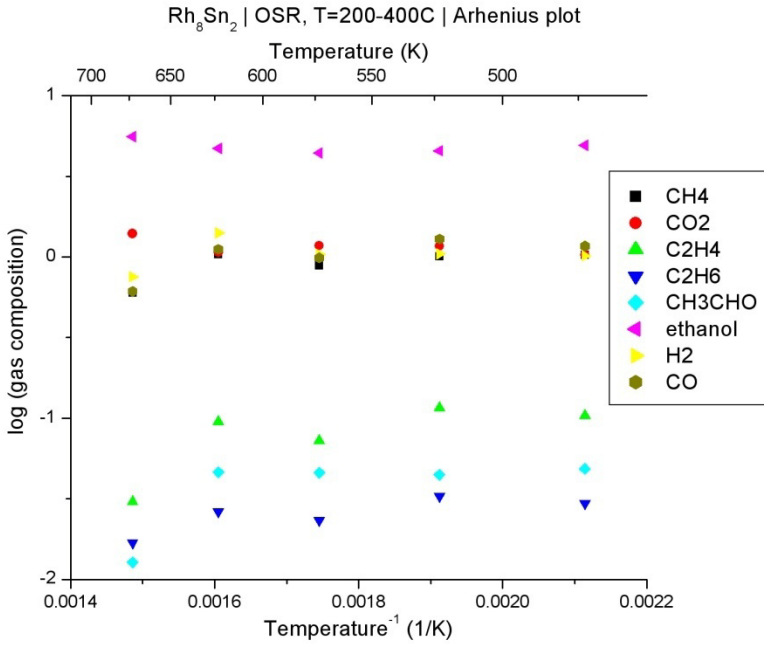

Figure 50: Arhenius plot of the product gas composition for oxidative steam reforming.

7.4 Ethanol Reforming over Pt (5% wt.)/CeO_2

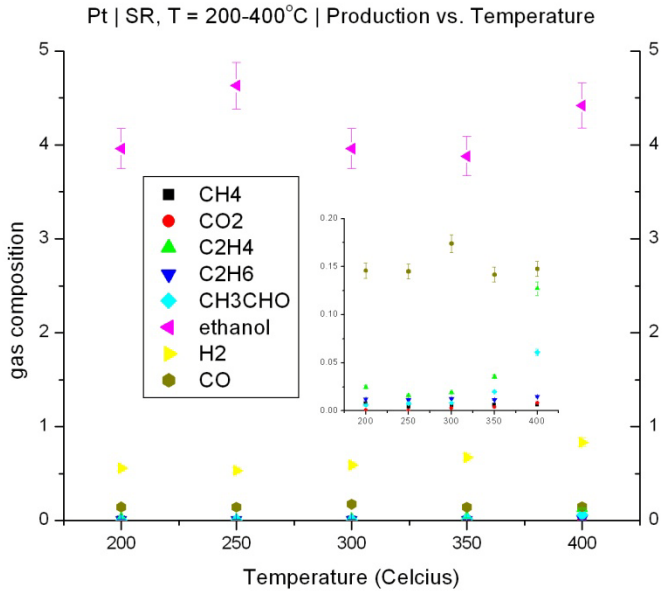

Figure 51: Product gas composition versus Temperature for steam reforming. Molar ratio of water-to-ethanol in the reactant gas is 3:1. The ratio of catalyst mass to reactant flow was 7.8 kg · sec/m was used, while ethanol vapor and steam flow rates were set at 10 and 31 sccm.

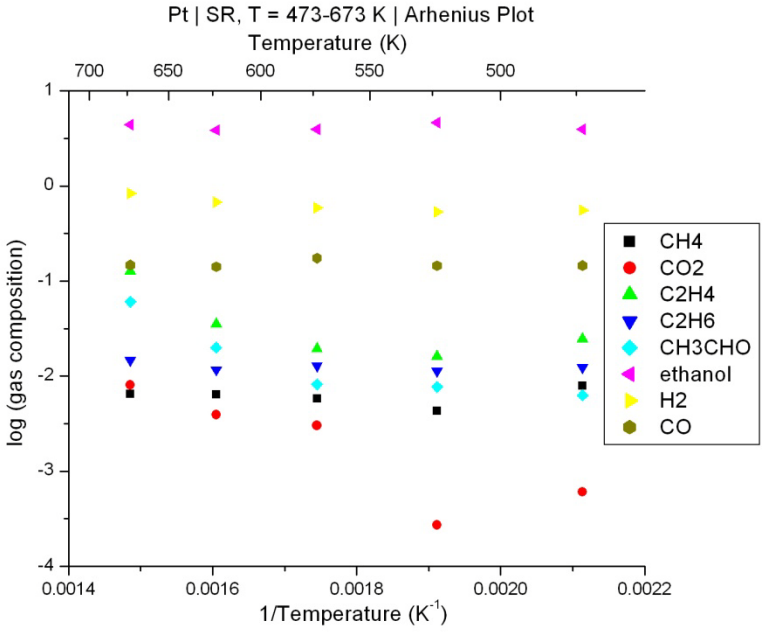

Figure 52: Arhenius plot of the product gas composition for steam reforming.

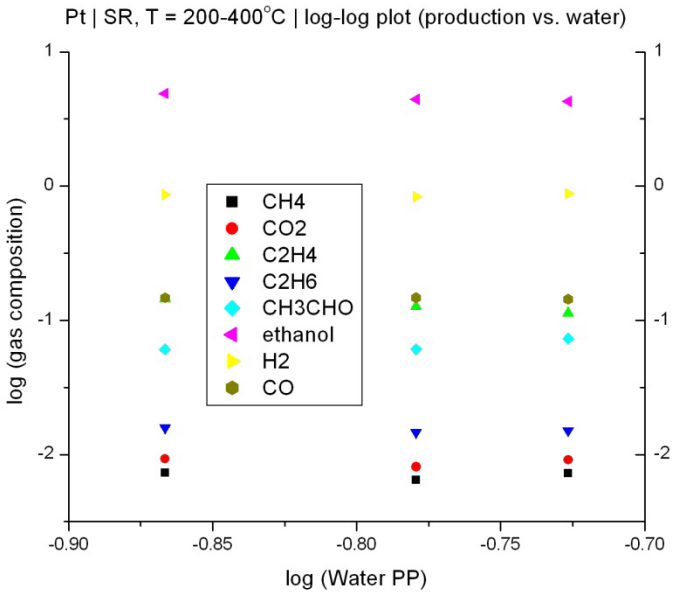

Figure 53: Log-log plot of product gas composition versus the inlet steam partial pressure. The ratio of catalyst mass to reactant flow was 6.2 – 10.4 kg · sec/m. Ethanol flow rate was held constant at 10.4 sccm.

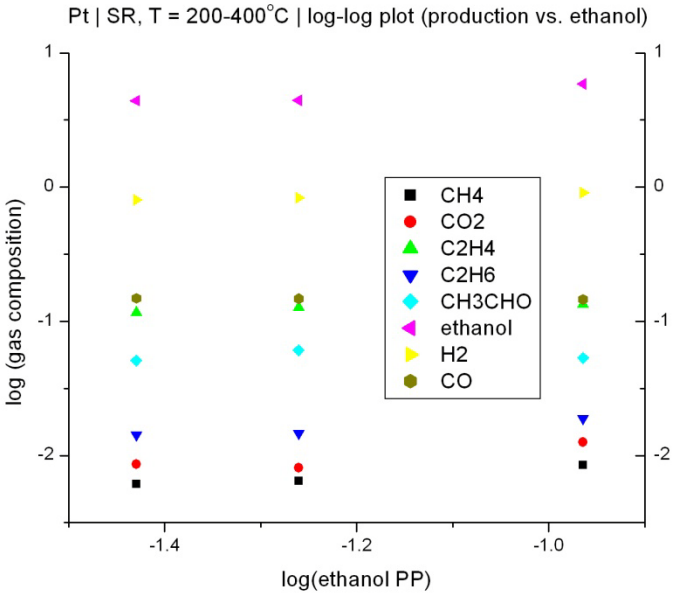

Figure 54: Log-log plot of product gas composition versus the inlet ethanol partial pressure. The ratio of catalyst mass to reactant flow was 7.2 – 8.5 kg · sec/m. Steam flow rate has held constant at 31.1 sccm.

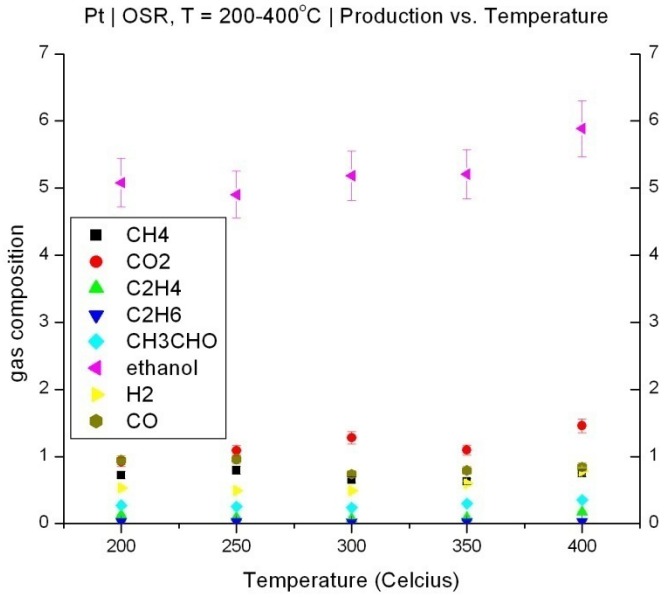

Figure 55: Product gas composition versus temperature for oxidative steam reforming. Molar ratio of Water-to-Ethanol-to-Oxygen in the reactant gas is 1.8:1.0:0.6. The ratio of catalyst mass to reactant flow was 6.1 kg · sec/m, while ethanol vapor, steam, oxygen and argon flow rates were set to 15.7, 28.2, 9.4 and 120 sccm, respectively.

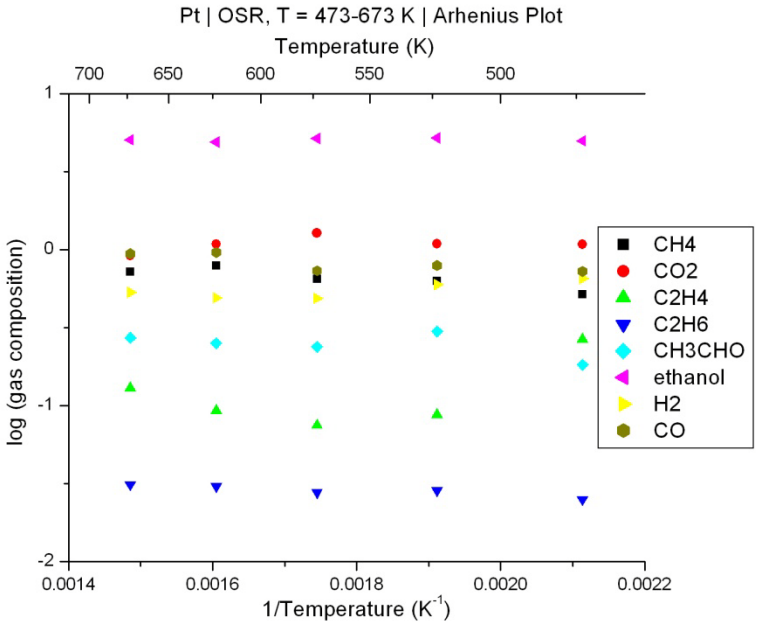

Figure 56: Arhenius plot of the product gas composition for oxidative steam reforming.

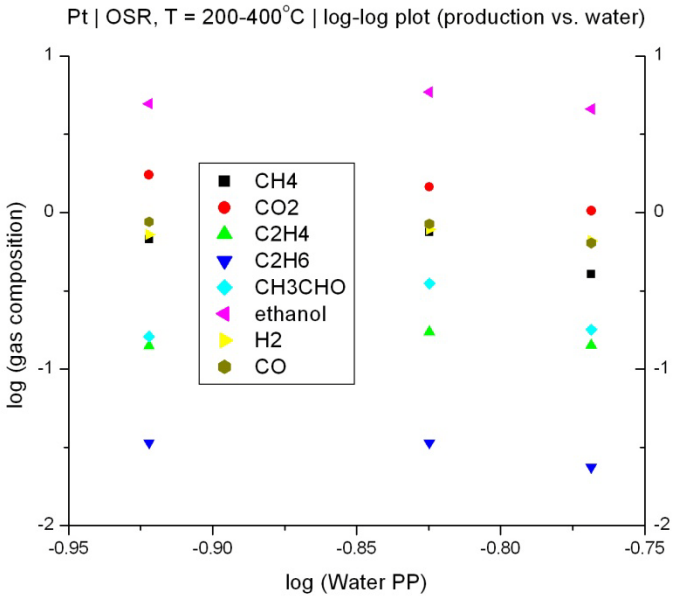

Figure 57: Log-log plot of product gas composition versus the inlet steam partial pressure. The ratio of catalyst mass to reactant flow was 5.2 – 7.4 kg · sec/m. Ethanol and oxygen flow rates were held constant at 9.4 and 15.7 sccm. The molar ratio of water:ethanol:oxygen in the reactant gas is 1.2-2.4:1:0.6.

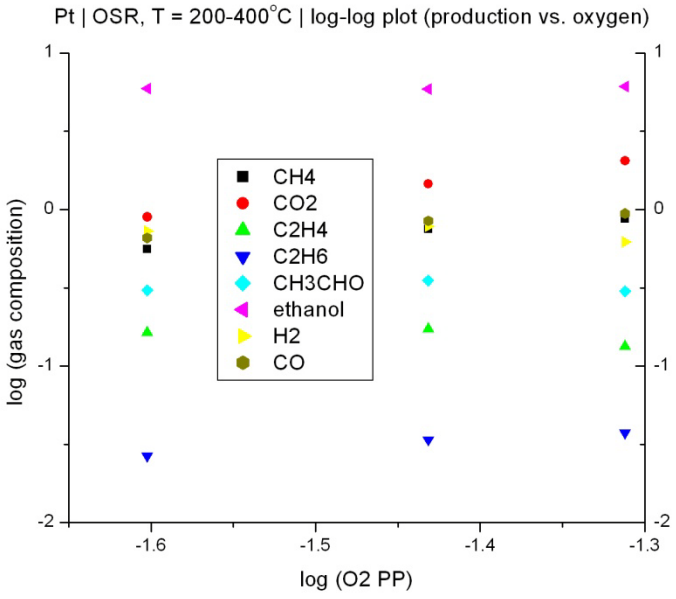

Figure 58: Log-log plot of product gas composition versus the inlet oxygen partial pressure. The ratio of catalyst mass to reactant flow was 5.7 – 6.3 kg · sec/m. Ethanol and steam flow rates were held constant at 15.7 and 28.2 sccm. The molar ratio of water:ethanol:oxygen in the reactant gas 1.8:1:0.4-0.8.

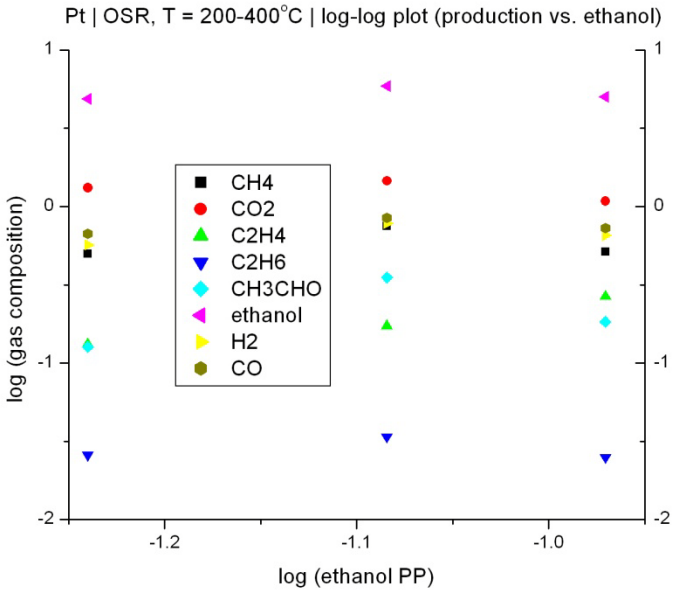

Figure 59: Log-log plot of product gas composition versus the inlet ethanol partial pressure. The ratio of catalyst mass to reactant flow was 5.5 – 6.7 kg · sec/m. Oxygen and steam flow rates were held constant at 9.4 and 28.2 sccm. The molar ratio of water:ethanol:oxygen in the reactant gas 1.8:1.33-0.66:0.6.

7.5 Ethanol Reforming over Pt_9Sn_1 (5% wt.)/CeO_2

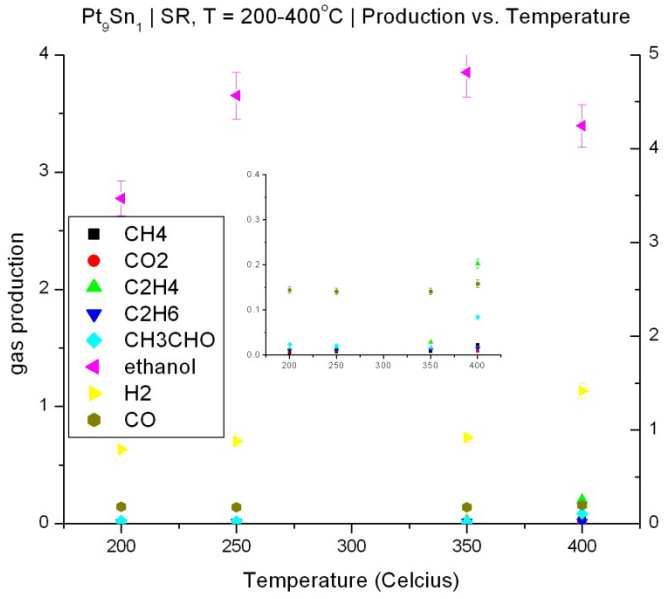

Figure 60: Product gas composition versus Temperature for steam reforming. Molar ratio of water-to-ethanol in the reactant gas is 3:1. The ratio of catalyst mass to reactant flow was 7.8 kg · sec/m, while ethanol vapor and steam flow rates were set at 10 and 31 sccm.

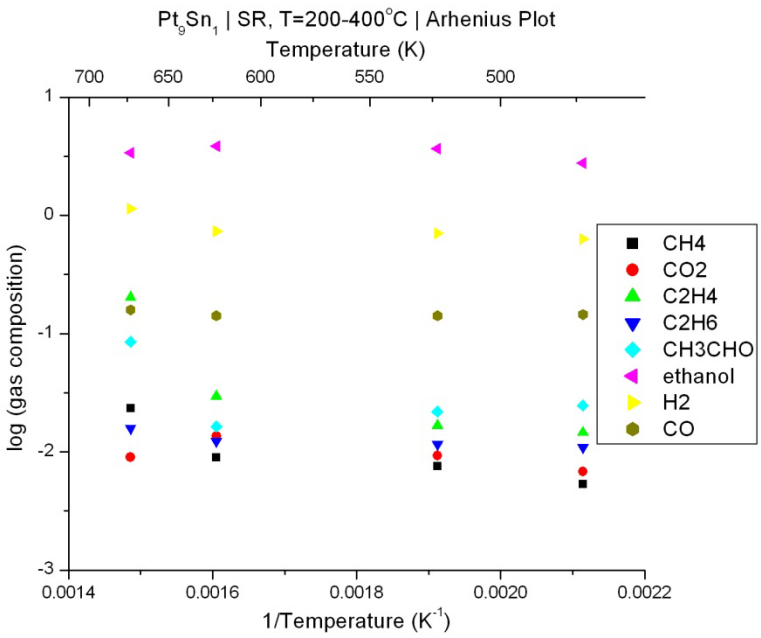

Figure 61: Arhenius plot of the product gas composition for steam reforming.

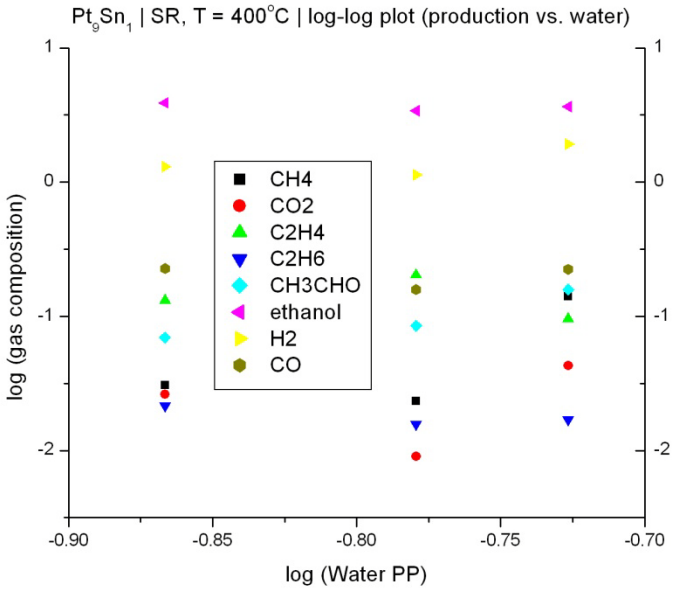

Figure 62: Log-log plot of product gas composition versus the inlet steam partial pressure. The ratio of catalyst mass to reactant flow was 6.2 – 10.4 kg · sec/m. Ethanol flow rate was held constant at 10.4 sccm.

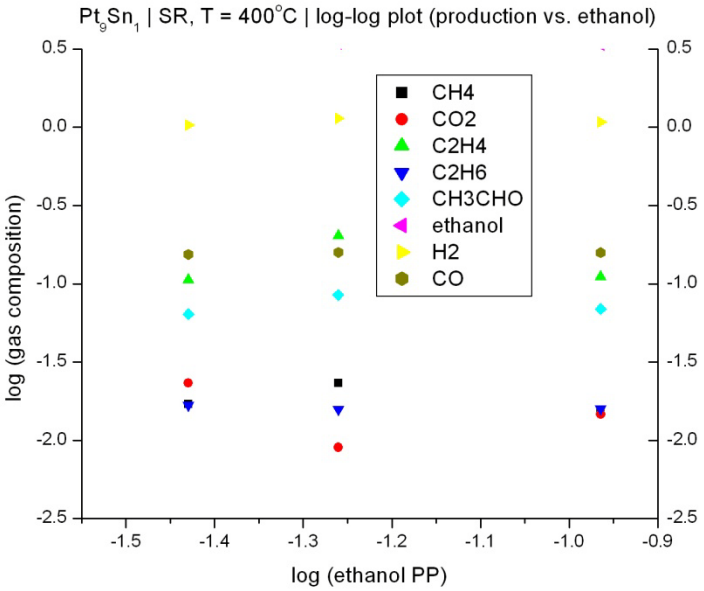

Figure 63: Log-log plot of product gas composition versus the inlet ethanol partial pressure. The ratio of catalyst mass to reactant flow was 7.2 – 8.5 kg · sec/m. Steam flow rate has held constant at 31.1 sccm.

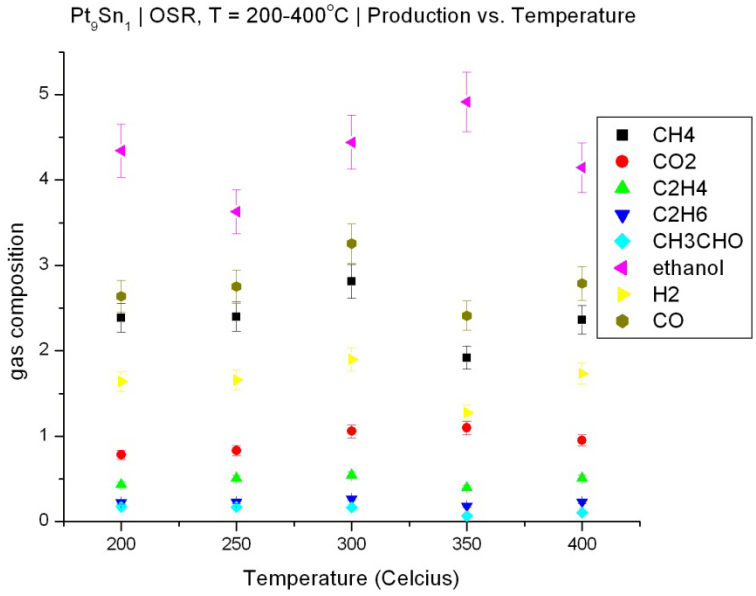

Figure 64: Product gas composition versus temperature for oxidative steam reforming. Molar ratio of water-to-ethanol-to-oxygen in the reactant gas is 1.8:1.0:0.6. The ratio of catalyst mass to reactant flow was 6.1 kg · sec /m^2, while ethanol vapor, steam, oxygen and argon flow rates were set to 15.7, 28.2, 9.4 and 120 sccm, respectively.

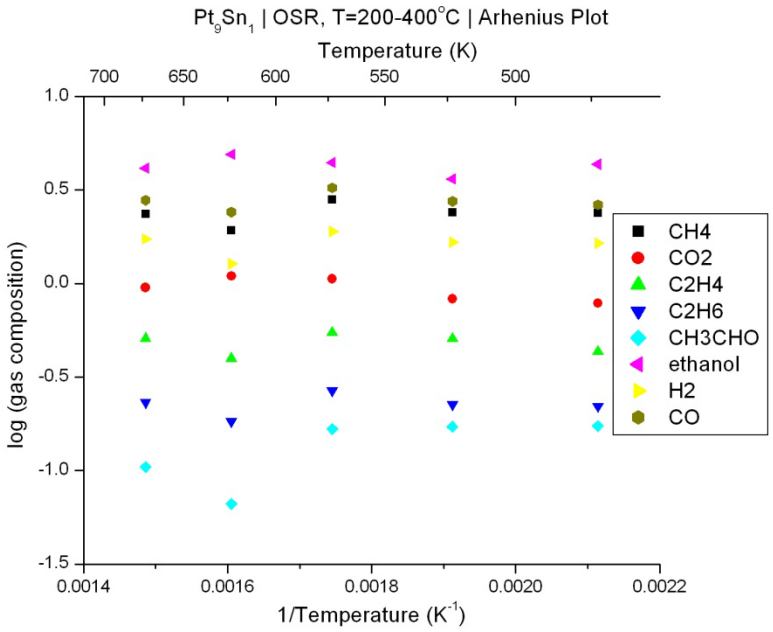

Figure 65: Arhenius plot of the product gas composition for oxidative steam reforming.

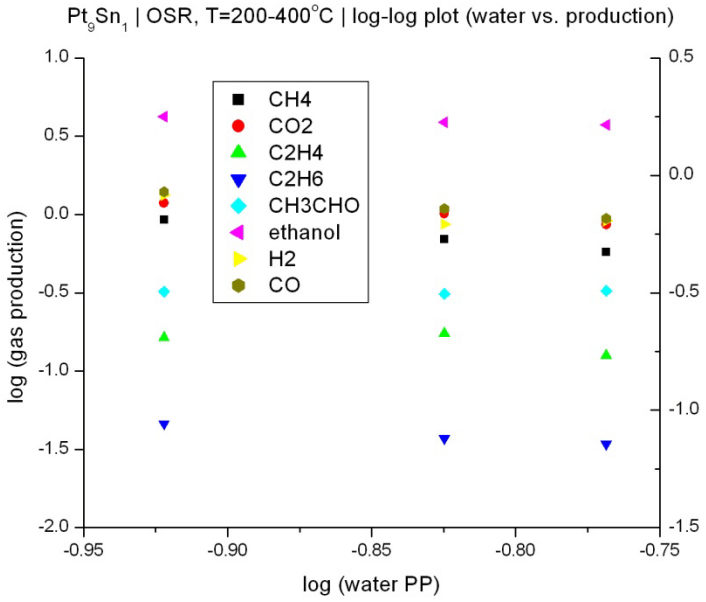

Figure 66: Log-log plot of product gas composition versus the inlet steam partial pressure. The ratio of catalyst mass to reactant flow was 5.2 – 7.4 kg · sec/m. Ethanol and oxygen flow rates were held constant at 9.4 and 15.7 sccm. The molar ratio of water:ethanol:oxygen in the reactant gas is 1.2-2.4:1:0.6.

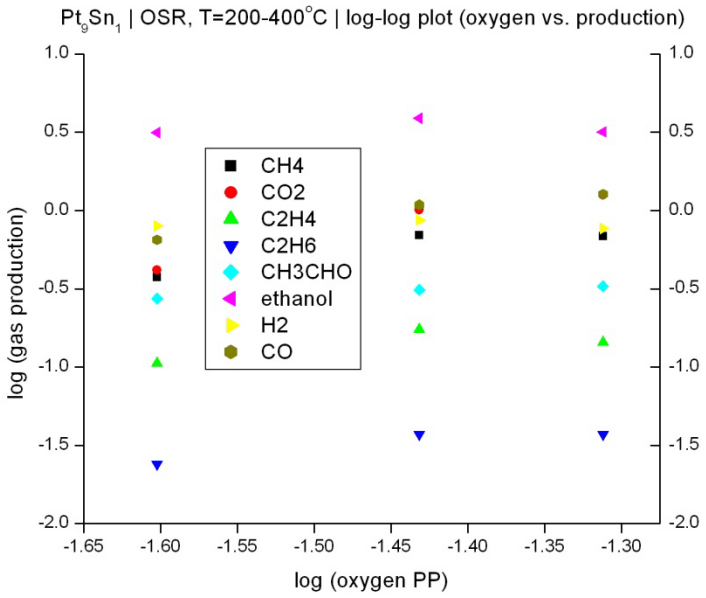

Figure 67: Log-log plot of product gas composition versus the inlet oxygen partial pressure. The ratio of catalyst mass to reactant flow was 5.7 – 6.3 kg · sec/m. Ethanol and steam flow rates were held constant at 15.7 and 28.2 sccm. The molar ratio of water:ethanol:oxygen in the reactant gas 1.8:1:0.4-0.8.

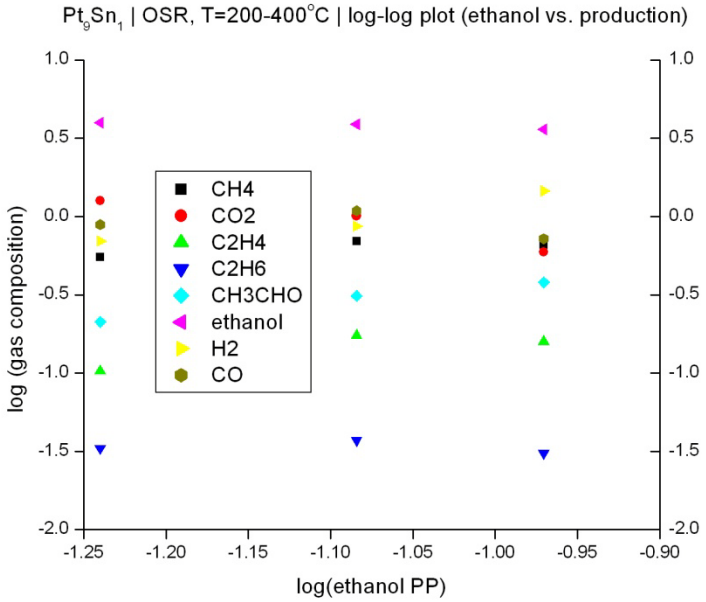

Figure 68: Log-log plot of product gas composition versus the inlet ethanol partial pressure. 5.5 – 6.7 kg · sec/m. oxygen and steam flow rates were held constant at 9.4 and 28.2 sccm. The molar ratio of water:ethanol:oxygen in the reactant gas 1.8:1.33-0.66:0.6.

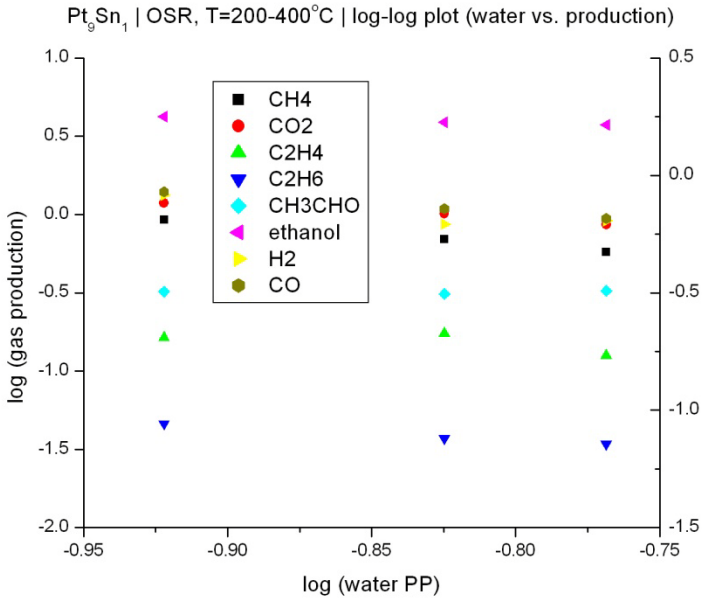

Figure 69: Log-log plot of product gas composition versus the inlet steam partial pressure. The ratio of catalyst mass to reactant flow was 5.2 – 7.4 kg · sec/m. Ethanol and oxygen flow rates were held constant at 9.4 and 15.7 sccm. The molar ratio of water:ethanol:oxygen in the reactant gas is 1.2-2.4:1:0.6.

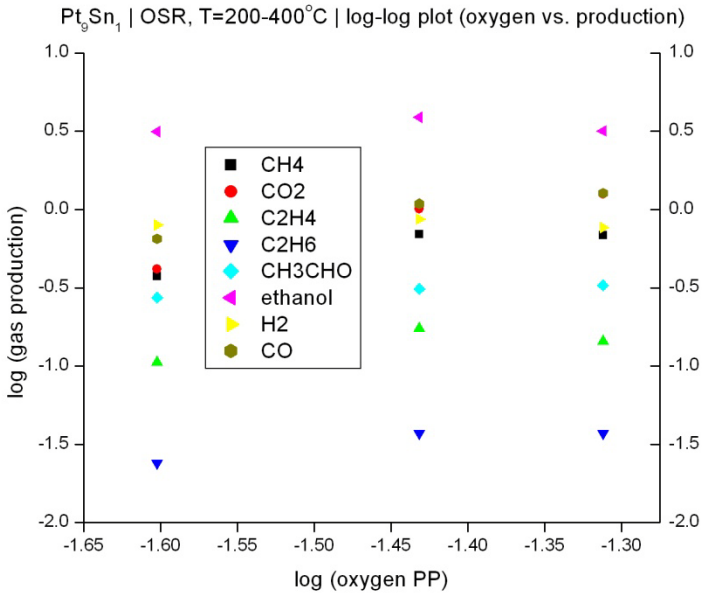

Figure 70: Log-log plot of product gas composition versus the inlet oxygen partial pressure. The ratio of catalyst mass to reactant flow was 5.7 – 6.3 kg · sec/m. Ethanol and steam flow rates were held constant at 15.7 and 28.2 sccm. The molar ratio of water:ethanol:oxygen in the reactant gas 1.8:1:0.4-0.8.

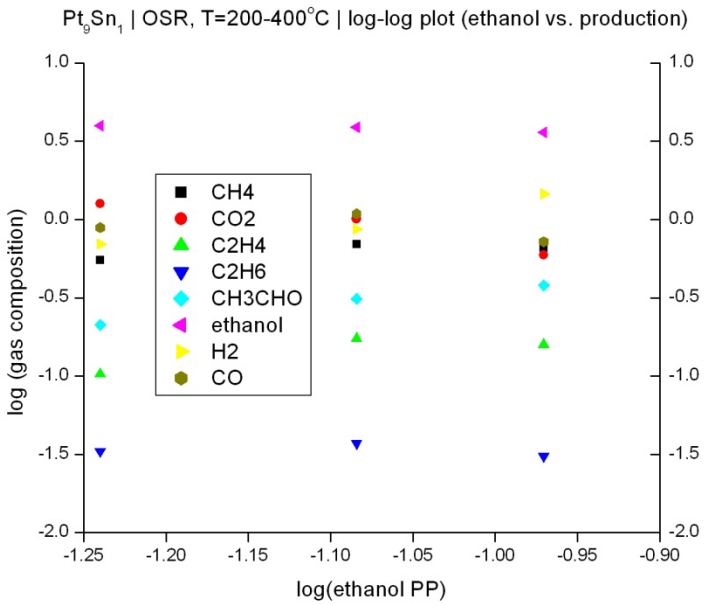

Figure 71: Log-log plot of product gas composition versus the inlet ethanol partial pressure. The ratio of catalyst mass to reactant flow was 5.5 – 6.7 kg · sec/m. Oxygen and steam flow rates were held constant at 9.4 and 28.2 sccm. The molar ratio of water:ethanol:oxygen in the reactant gas 1.8:1.33-0.66:0.6.

7.6 Ethanol Reforming over Pt_8Sn_2 (5% wt.)/CeO_2

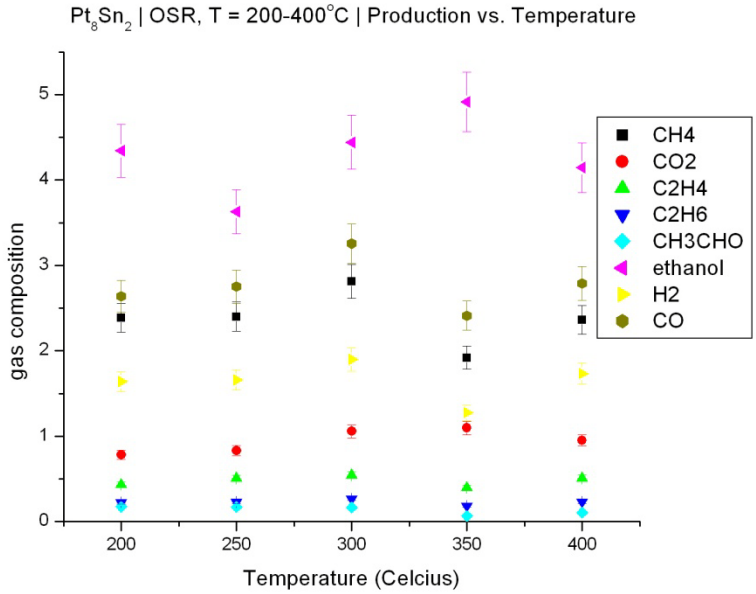

Figure 72: Product gas composition versus Temperature for steam reforming. Molar ratio of water-to-ethanol in the reactant gas is 3:1. The ratio of catalyst mass to reactant flow was 7.8 kg · sec/m, while ethanol vapor and steam flow rates were set at 10 and 31 sccm.

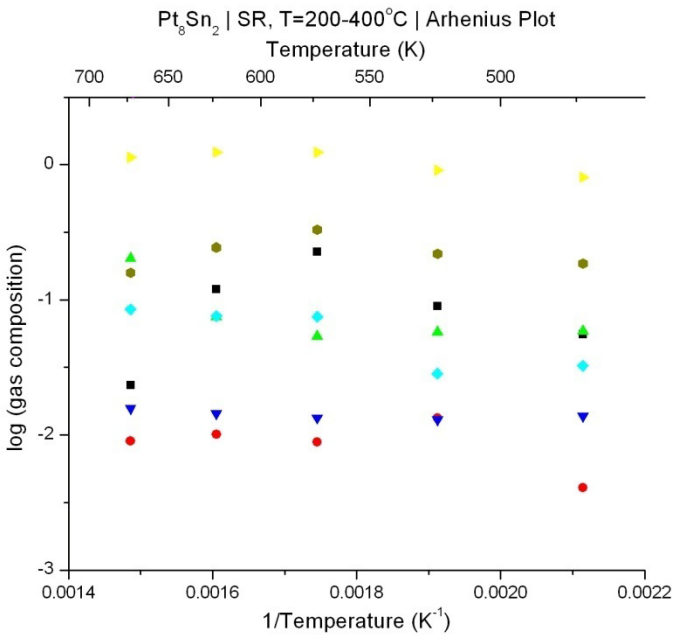

Figure 73: Arhenius plot of the product gas composition for steam reforming.

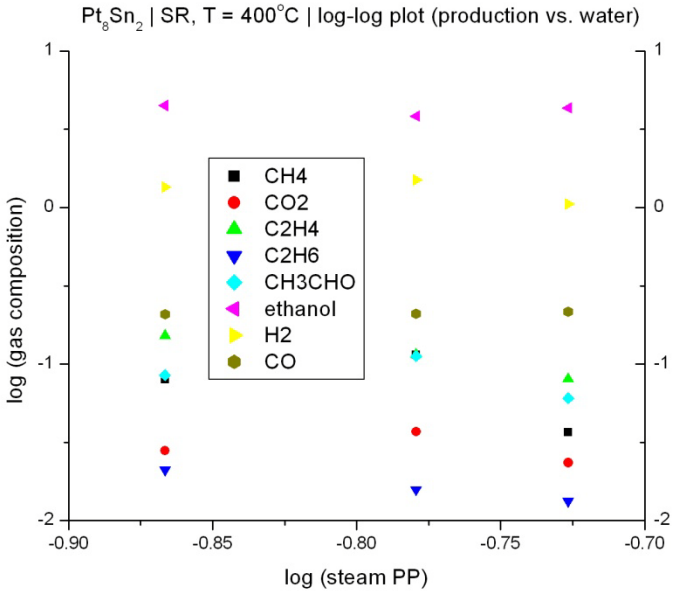

Figure 74: Log-log plot of product gas composition versus the inlet steam partial pressure. The ratio of catalyst mass to reactant flow was 6.2 – 10.4 kg · sec/m. Ethanol flow rate was held constant at 10.4 sccm.

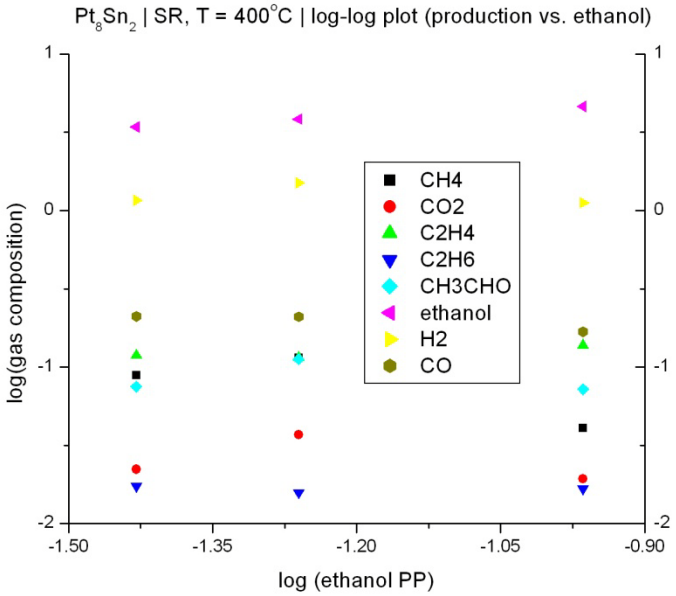

Figure 75: Log-log plot of product gas composition versus the inlet ethanol partial pressure. The ratio of catalyst mass to reactant flow was 7.2 – 8.5 kg · sec/m. Steam flow rate has held constant at 31.1 sccm.

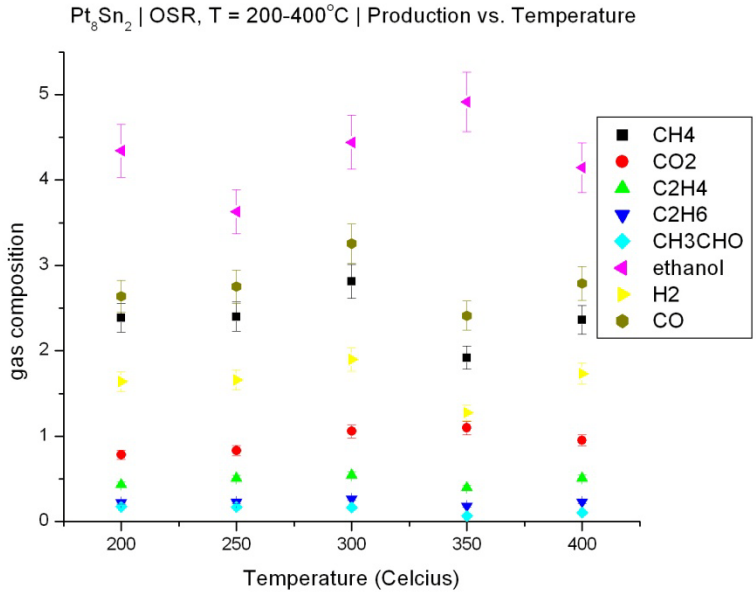

Figure 76: Product gas composition versus temperature for oxidative steam reforming. Molar ratio of Water-to-ethanol-to-oxygen in the reactant gas is 1.8:1.0:0.6. The ratio of catalyst mass to reactant flow was 6.1 kg · sec/m, while ethanol vapor, steam, oxygen and argon flow rates were set to 15.7, 28.2, 9.4 and 120 sccm, respectively.

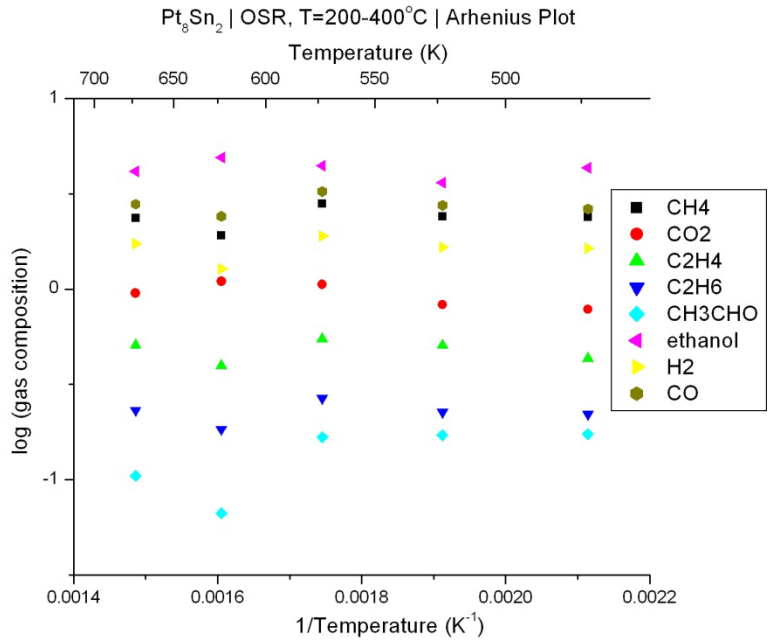

Figure 77: Arhenius plot of the product gas composition for oxidative steam reforming.

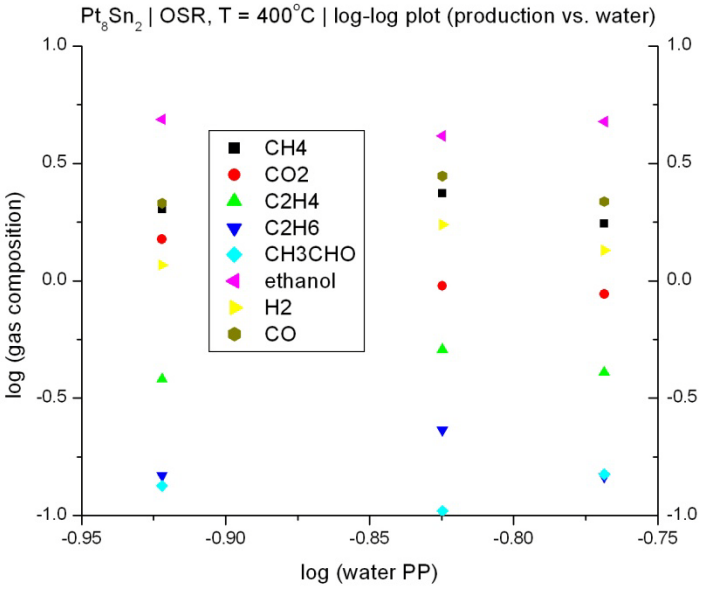

Figure 78: Log-log plot of product gas composition versus the inlet steam partial pressure. The ratio of catalyst mass to reactant flow was 5.2 – 7.4 kg · sec/m. Ethanol and oxygen flow rates were held constant at 9.4 and 15.7 sccm. The molar ratio of water:ethanol:oxygen in the reactant gas is 1.2-2.4:1:0.6.

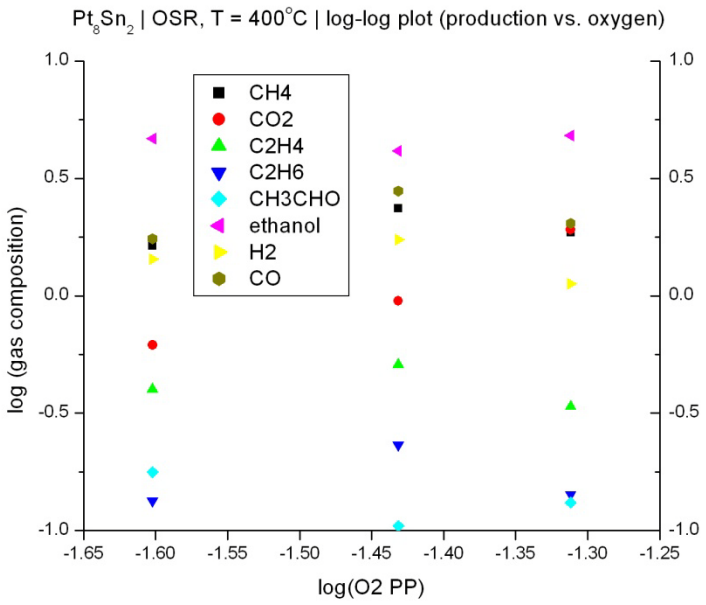

Figure 79: Log-log plot of product gas composition versus the inlet oxygen partial pressure. The ratio of catalyst mass to reactant flow was 5.7 – 6.3 kg · sec/m. Ethanol and steam flow rates were held constant at 15.7 and 28.2 sccm. The molar ratio of water:ethanol:oxygen in the reactant gas 1.8:1:0.4-0.8.

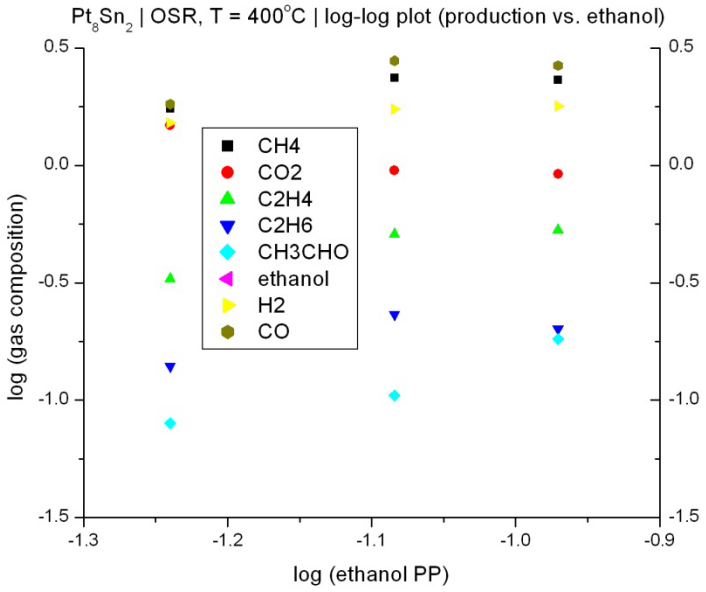

Figure 80: Log-log plot of product gas composition versus the inlet ethanol partial pressure. The ratio of catalyst mass to reactant flow was 5.5 – 6.7 kg · sec/m. Oxygen and steam flow rates were held constant at 9.4 and 28.2 sccm. The molar ratio of water:ethanol:oxygen in the reactant gas 1.8:1.33-0.66:0.6.

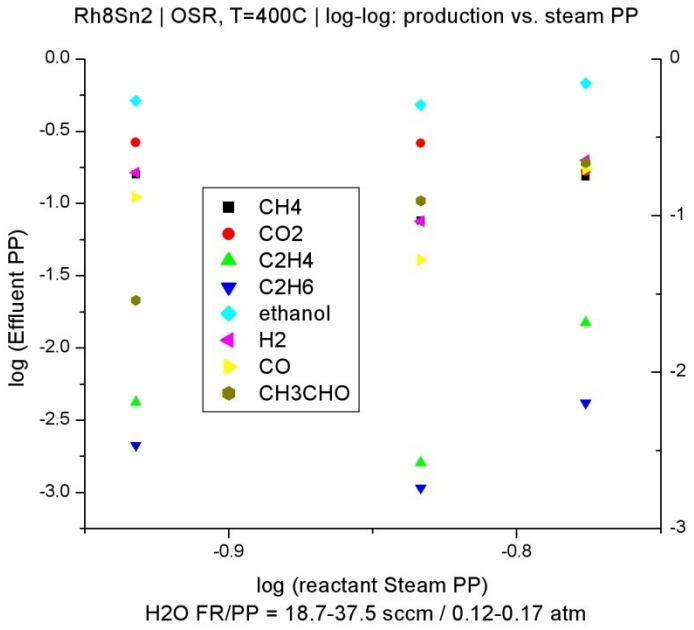

Figure 81: Log-log plot of product gas composition versus the inlet steam partial pressure. The ratio of catalyst mass to reactant flow was 5.2 – 7.4 kg · sec/m. Ethanol and oxygen flow rates were held constant at 9.4 and 15.7 sccm. The molar ratio of water:ethanol:oxygen in the reactant gas is 1.2-2.4:1:0.6.

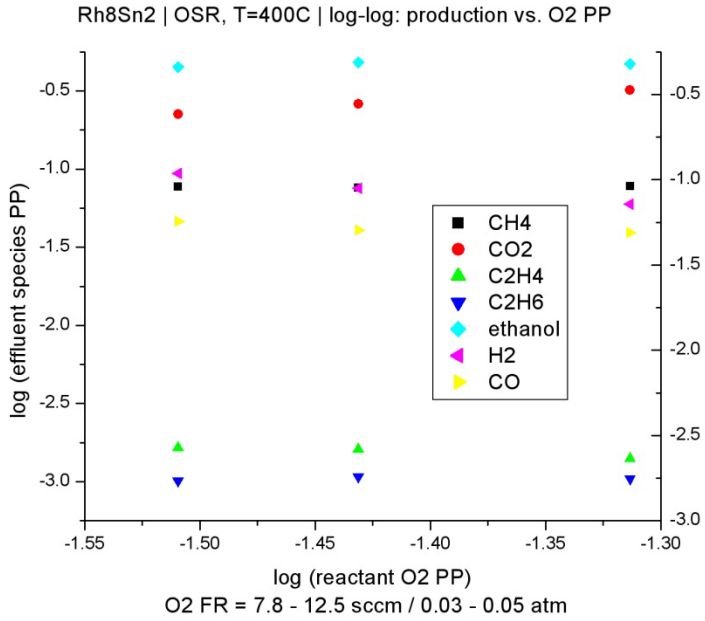

Figure 82: Log-log plot of product gas composition versus the inlet oxygen partial pressure. The ratio of catalyst mass to reactant flow was 5.7 – 6.3 kg · sec/m. Ethanol and steam flow rates were held constant at 15.7 and 28.2 sccm. The molar ratio of water:ethanol:oxygen in the reactant gas 1.8:1:0.4-0.8.

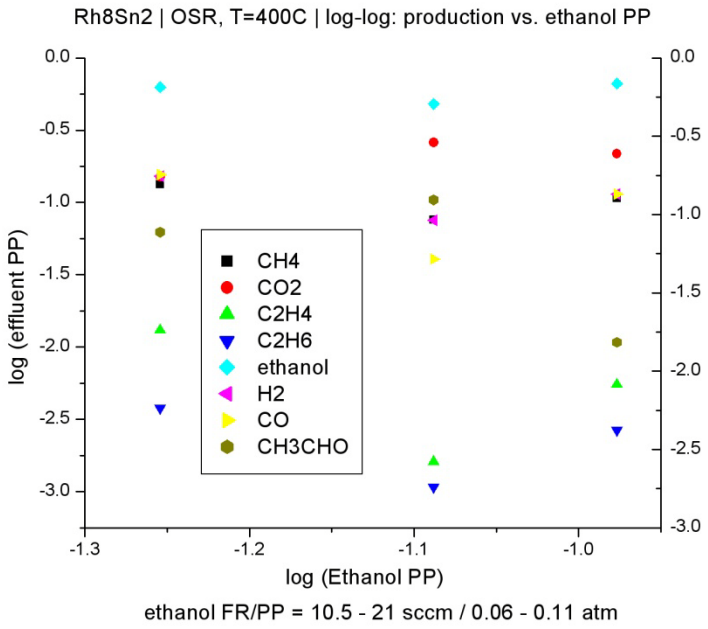

Figure 83: Log-log plot of product gas composition versus the inlet ethanol partial pressure. The ratio of catalyst mass to reactant flow was 5.5 – 6.7 kg · sec/m. Oxygen and steam flow rates were held constant at 9.4 and 28.2 sccm. The molar ratio of water:ethanol:oxygen in the reactant gas 1.8:1.33-0.66:0.6